Applied Clay Science 112–113 (2015) 75–93

Contents lists available at ScienceDirect

Applied Clay Science

journal homepage: www.elsevier.com/locate/clay

Review article

Properties and applications of halloysite nanotubes: recent research advances and future prospects

Peng Yuan [a,d,*], Daoyong Tan [b], Faïza Annabi-Bergaya [c]

[a] CAS Key Laboratory of Mineralogy and Metallogeny, Guangzhou Institute of Geochemistry, Chinese Academy of Sciences, Guangzhou 510640, China
[b] Key Laboratory of Solid Waste Treatment and Resource Recycle, Ministry of Education, Southwest University of Science and Technology, Mianyang 621010, China
[c] Centre de Recherche sur la Matière Divisée, CNRS-Université d'Orléans, Orléans 45071, France
[d] Guangdong Provincial Key Laboratory of Mineral Physics and Materials, Guangzhou 510640, China

ARTICLE INFO

Article history:
Received 9 March 2015
Received in revised form 30 April 2015
Accepted 3 May 2015
Available online xxxx

Keywords:
Halloysite nanotube (HNT)
Controlled release
Clay–polymer nanocomposite (CPN)
Adsorption
Modification
Hybrid nanomaterials

ABSTRACT

Halloysite is a natural nanosized tubular clay mineral that has many potentially important uses in different industrial fields. In this paper, the key structural characteristics and properties of halloysite and their related applications are comprehensively reviewed. Research advances on halloysite, especially those from the past 20 years, are summarized with some critical comments. Attention is mainly paid to the structure and morphology of halloysite and their changes, the formation of tubular structures, the physicochemical properties, the surface chemical modifications, and the halloysite-based advanced materials and some related applications. Additionally, future prospects and key problems to be solved in halloysite studies are discussed. This review shed new light on both fundamental and applied studies that focused on halloysite.

1. Introduction

Nanosized tubular halloysite, also called halloysite nanotube (HNT) in some materials science publications, is the dominant form of naturally occurring halloysite. It was first described by Berthier (1826) as a dioctahedral 1:1 clay mineral of the kaolin group. The multilayer tubular structure of halloysite results from the wrapping of the 1:1 clay mineral layers under favorable geological conditions, driven by a mismatch in the oxygen-sharing tetrahedral and octahedral sheets in the 1:1 layer (Bates et al., 1950; Singh, 1996). Halloysite is chemically similar to kaolinite, but the unit layers in halloysite are separated by a monolayer of water molecules; accordingly, halloysite has a structural formula of $Al_2(OH)_4Si_2O_5 \cdot nH_2O$. The hydrated form of halloysite (when $n = 2$) is named "halloysite-(10 Å)", in which one layer of water molecules is present between the multilayers and where the "10 Å" designation indicates the d_{001}-value of the layers. The dehydrated structure of halloysite (when $n = 0$) is named "halloysite-(7 Å)", and may be obtained through the loss of the interlayer water molecules under mild heating and/or a vacuum environment (Joussein et al., 2005). A schematic diagram of the structure of halloysite-(10 Å) is shown in Fig. 1. In this paper, "halloysite" is used hereafter for simplicity, regardless of hydration or dehydration, unless otherwise noted and will be abbreviated "Hal".

Worldwide, large Hal deposits have been found in Australia, the United States, China, New Zealand, Mexico, and Brazil (Joussein et al., 2005). However, the overall yield of Hal is much lower than the huge production of kaolinite (which will be abbreviated Kaol in this review). Natural Hal often contains impurity phases and varies in morphology and porosity in the different deposits (Pasbakhsh et al., 2013). In general, Hal nanotubes vary in length from the submicron scale to several microns, sometimes even >30 μm (Joussein et al, 2005), in external diameter from approximately 30 to 190 nm, and in internal diameter from approximately 10 to 100 nm (Yuan et al., 2008, 2013).

In the past decade, again Hal became a focus of many studies and patents, although its nanoscale structure had been identified already since few decades (Bates et al., 1950) *via* spectroscopic methods. This renewed interest should be ascribed to the rapid developments of nanoscience and nanotechnology in the past two decades, which drive the increasing interest on naturally occurring nanometric structures. Natural Hal exhibits several advantages in applications over synthetic nanotubes such as carbon nanotube (CNT). According to Lvov et al. (2008), Hal is a low-cost material (at about $4 per kg though the purification process could arise the price of raw ores, and this cost is much less expensive in developed countries) and its global supply exceeds thousands of tons per year, meaning that true mass-scale industrial applications can readily be achieved, unlike the gram-scale yielding of CNT with a very high price ($500 per kg). Furthermore, the advantage

* Corresponding author at: Guangzhou Institute of Geochemistry, Chinese Academy of Sciences Wushan, Guangzhou 510640, China. Tel./fax: +86 20 85290341.
E-mail address: yuanpeng@gig.ac.cn (P. Yuan).

http://dx.doi.org/10.1016/j.clay.2015.05.001
0169-1317/

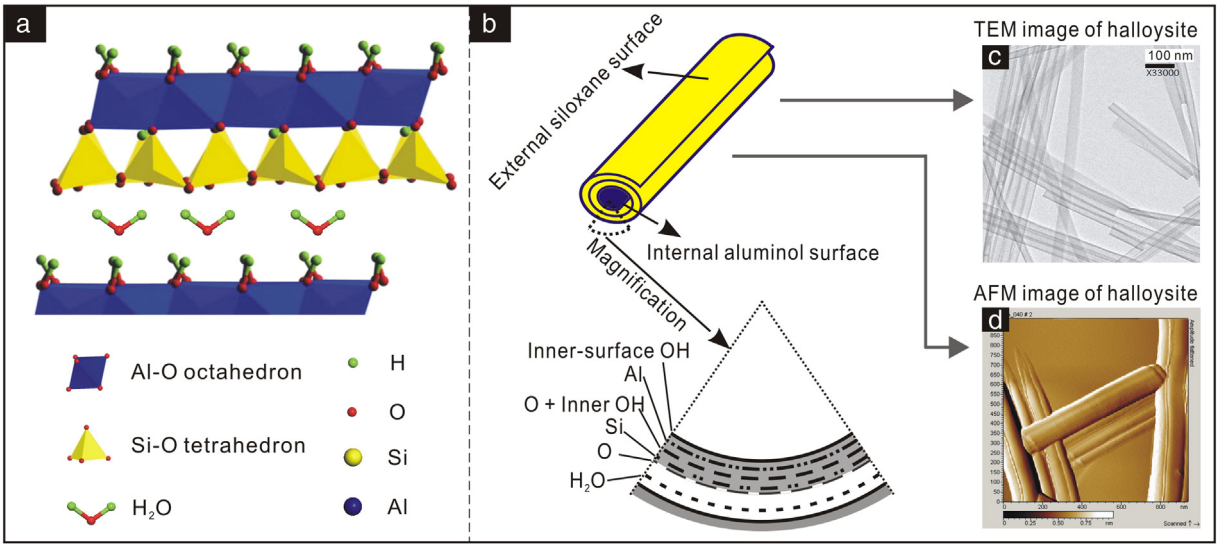

Fig. 1. Schematic diagram of (a) crystalline structure of Hal-(10 Å), (b) structure of Hal particle, (c–f) TEM and AFM images of Hal.

of Hal is not limited to its economic viability. Hal possesses a one-dimensional tubular porous structure on the mesoporous (2–50 nm) and even macroporous (>50 nm) scale (Churchman et al., 1995), which is larger than many synthetic porous materials such as CNT. This property enables versatile potential applications such as nanoscale support for the loading of functional guests; for example, a mesoporous lumen may enable Hal availability for the immobilization of large-sized enzymes, *e.g.*, serum albumin and conalbumin, which cannot even be hosted by SBA-15 (Yiu et al., 2001). In addition, the unique tubular structure of Hal is combined with site-dependent aluminosilicate chemistry, *i.e.*, the reactivity of the external surface, the internal lumen surface, and the interlayer surface of Hal is different, thus enabling abundant possibilities for the post-modification of Hal targeted for various applications (Yuan et al., 2008). It is also worth emphasizing that Hal has a high biocompatibility and low cytotoxicity, which promises its safe use in various fields (Vergaro et al., 2010).

Some very interesting research advances focusing on the novel properties and related applications of Hal have been successively reported in the past 20 years. For example, the use of Hal as a viable nanoscale container for the encapsulation of biologically active molecules such as biocides and drugs as well as for their controlled release was first demonstrated by Price et al. (2001), and Hal as a nanofiller in clay–polymer nanocomposites (CPN) was proposed (Du et al., 2006). Concerning the formation of Hal, Gardolinski and Lagaly (2005) proposed a multistep intercalation of Kaol for the transformation of platy Kaol to Hal-like nanotubes and Kuroda et al. (2011) recently proposed a simple one-step preparation of Hal-like nanotube through the delamination and rolling of Kaol. In addition, some key fundamental properties of Hal, such as structural stability under heating (Yuan et al., 2012a) or in acidic/alkaline aqueous dispersions (White et al., 2012) and site-specific availability for surface organosilane grafting modification (Yuan et al., 2008), were comprehensively investigated.

In view of the abovementioned research advances, there are great prospects for Hal-based materials. In this regard, a comprehensive and critical review on previous Hal studies is no doubt necessary and might constitute a premise for a better understanding of the specificity of Hal. Accordingly, the objective of this review is to outline the primary properties of the structure and reactivity of Hal as well as related applications by collating the disparate results from the literature. Moreover, some critical assessments on the collated results or discussions on related prospects are made to initiate possible new ideas in the future. The main focus of this review is directed to the research advances of the past decade because earlier advances have been comprehensively summarized by Joussein et al. (2005). In addition, topics such as the geological genesis and morphology/structure diversity of natural Hal are briefly reviewed because they have already been detailed in the literature.

2. Geological occurrence of halloysite (Hal)

Generally, Hal can be derived by the weathering, pedogenesis or hydrothermal alteration of ultramafic rocks, volcanic glass, and pumice (Joussein et al., 2005). The main geological occurrence of Hal is in weathered or hydrothermally altered rocks, saprolites, and soils. With different genesis, Hal is accompanied by different types of associated minerals. For instance, the Matauri Bay Hal deposit (in Northland, New Zealand), formed by the low temperature hydrothermal alteration of rhyolite and dacite volcanic rocks, is mainly associated with quartz, cristobalite, and feldspar. The Dragon Mine Hal deposit (in Utah, USA), formed by the hydrothermal alteration of dolomite, is associated with Kaol, gibbsite, alunite, and quartz (Pasbakhsh et al., 2013). In addition, the crystallization conditions and geological occurrence of Hal are closely related to its morphology. For example, the Hal exhibits spheroidal morphology when recrystallized from supersaturated solutions of volcanic glass and pumice (Joussein et al., 2005); however, the Hal exhibits a tubular morphology when formed by the hydrothermal alteration of biotite (Papoulis et al., 2009), by the weathering of feldspar in granitic rocks (Adamo et al., 2001), and by the topological alteration of platy Kaol (Singh and Gilkes, 1992). More details concerning the geological genesis of Hal can be found in previous reports (Joussein et al., 2005; Pasbakhsh et al., 2013).

3. Structure and morphology of halloysite (Hal)

3.1. Mechanism of tubular structure formation of Hal

Naturally occurring Hal appears in varied morphologies, such as platy, spheroidal, and tubular. However, the tubular structure is the dominant morphology of Hal in nature. The formation of the tubular structure is triggered by atomic-scaled stress in the unit layer of Hal, which is originally caused by the mismatch in the larger tetrahedral ($a = 5.02$ Å, $b = 9.164$ Å) and the smaller octahedral ($a = 5.066$ Å, $b = 8.655$ Å) sheets (Bates et al, 1950; Bailey, 1990). Because these octahedral and tetrahedral sheets are connected by sharing the apical oxygen of the tetrahedron, the stretched Al–O bond in the octahedron could constrain the shared apical oxygen and induce structural stress

in the plane of the apical oxygen (or in the plane of the inner hydroxyl). This induced stress is transmitted through Si–O covalent bonds to the Si plane and the basal oxygen plane but is attenuated by the angular flexibility of the Si–O bonds. The structural stress of Hal can be generated on the plane of the basal oxygen and also on the plane of the apical oxygen (Singh, 1996).

In the case of hydrated Hal, the stress on the plane of the basal oxygen is readily relieved by the separation of the layers because of the presence of interlayer water molecules. However, the stress on the plane of the apical oxygen, lying in the middle of the unit layer, is hardly affected by the interlayer water molecules. To compensate this stress, Hal adopts both a rotation of the tetrahedron and a rolling of the unit layer (Fig. 2) to correct the mismatch between the plane of the apical oxygen and the plane of the inner hydroxyl and merges them into a single plane. In the rotation mechanism, adjacent tetrahedrons rotate in opposite directions to reduce the lateral dimension of the tetrahedral sheet by shrinking the distances to an equal value for the basal oxygen, silicon, and the apical oxygen in all directions in the *ab* plane. Consequently, the configuration of the tetrahedral sheet is transformed from hexagonal to ditrigonal. In the rolling mechanism, the constriction occurs only along the rolled axis and the apical oxygen located relatively more inside the curvature than the Si and basal oxygen, could generate a greater constriction and therefore adjust the mismatch with a higher efficiency than the rotation mechanism. Generally, the natural Hal first undergoes the more efficient rolling mechanism to relieve the stress to the maximum extent and then undergoes the tetrahedral rotation to compensate the residual stress (Singh, 1996). The long axis of natural Hal is predominantly parallel to the *b* axis, and partially parallel to the *a* axis (Honjo et al., 1954; Singh and Gilkes, 1992), which means that the orientation of rolling/curling is [100] and [010], respectively. This phenomenon also occurs in synthetic Hal-like nanotubes (Singh and Mackinnon, 1996; Kuroda et al, 2011). In addition to the abovementioned curling orientations, Niu et al. (2014) found that there were four new curling orientations, [1$\bar{1}$0], [110], [310], and [3$\bar{1}$0], and that these multiple curling orientations were ascribed to the incompatible matching between tetrahedrons and octahedrons, and to the hexagonal distributions and the *zigzag* distributions of two matching types (two-one type and two-two type).

In the case of platy Kaol, the structural stress is effectively compensated by the formation of hydrogen bonds between the basal oxygen and the inner-surface hydroxyl of the adjacent layer. Based on this theory, the obtention of Hal through rolling of the Kaol layers by weakening the interlayer hydrogen bonds attracted much interest. Singh and Mackinnon (1996) experimentally demonstrated the formation of Hal-like nanotubes through the use of repeated intercalation and deintercalation of Kaol using potassium acetate. Gardolinski and Lagaly (2005) proposed a method for the transformation of platy Kaol to Hal-like nanotubes with high transformation efficiency, where the interlayer-grafted Kaol was intercalated with n-alkylamines and deintercalated by toluene, and the rolling of thin Kaol particles was observed. Using the same method, Matusik et al. (2009) investigated the effect of the structural order of the parent Kaol on the formation of Hal-like nanotubes and found that the production of nanotubes primarily depends on the efficiency of the interlayer modification and on the low crystallinity of the Kaol. The preparation of Hal-like nanotubes through the delamination and rolling of Kaol was further developed by Kuroda et al. (2011), who proposed a simple one-step method where some quaternary ammonium salts, such as hexadecyl trimethylammonium chloride and dodecyl trimethylammonium bromide, were intercalated in the interlayer space of methoxy-modified Kaol. The trimethylammonium group of the intercalated guest interacted weakly with the tetrahedral sheets of Kaol, inducing the formation of a flexible array of intercalated guest for swelling and the concurrent transformation of platy Kaol to nanotubes. This transformation was quite dependent on the interaction between the intercalated guests and the interlayer surface of the methoxy-modified Kaol. If this interaction is too weak, the intercalation of the guest is hard; if this interaction was too strong, the transformation *via* one-step cannot be accomplished because of the formation of a rigid array of intercalated guests. Instead, this transformation was accomplished *via* two-step in which the intercalation and swelling proceed separately (Fig. 3). Yuan et al. (2013) investigated the effect of intercalation reaction parameters, including temperature, time, and concentration of quaternary ammonium salts, on the transformation of platy Kaol to Hal-like nanotubes. Overall, the synthesized Hal-like nanotubes are of high tubule quality with uniform morphology, and could be used in industrial fields as alternatives to natural Hal, the performance of which is often affected by the diverse quality of the natural Hal sourced from different deposits. However, the large-scale production of Hal through the delamination and rolling of Kaol remains limited by the economic viability of this route.

3.2. Morphology and porous structure of Hal

The morphological parameters of Hal (length, internal/external diameter, ratio, and tube thickness) vary significantly between and even within deposits, as summarized in Table 1, and this diversity is due to the formation of Hal under various crystallization conditions and geological occurrences (Joussein et al., 2005; Yuan et al., 2008; Pasbakhsh et al., 2013). For example, Hal sourced from Kalgoorlie in Western Australia is thin-walled and highly uniform in length, diameter, and morphology; Hal sourced from Camel Lake in South Australia is thick-walled and has a relatively uniform morphology with good tubule quality; and Hal sourced from Northland in New Zealand has a

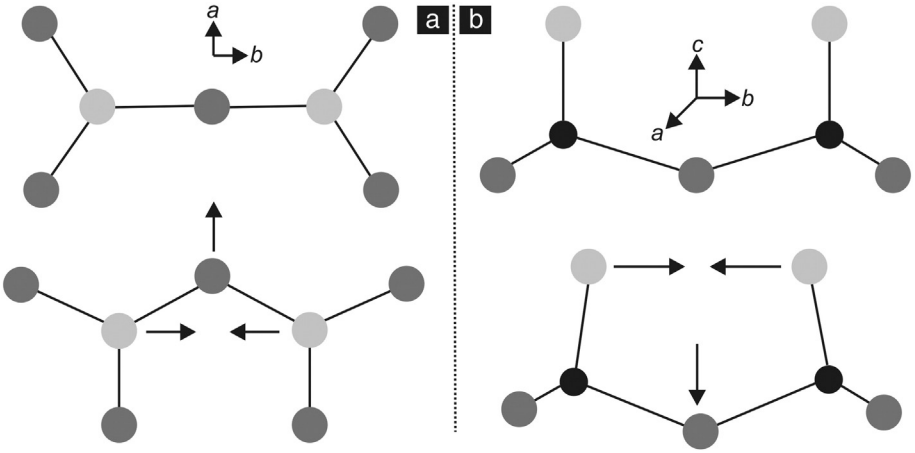

Fig. 2. (a) Rotation and (b) rolling mechanisms of tetrahedral in Hal. Adapted from Singh (1996) with permission.

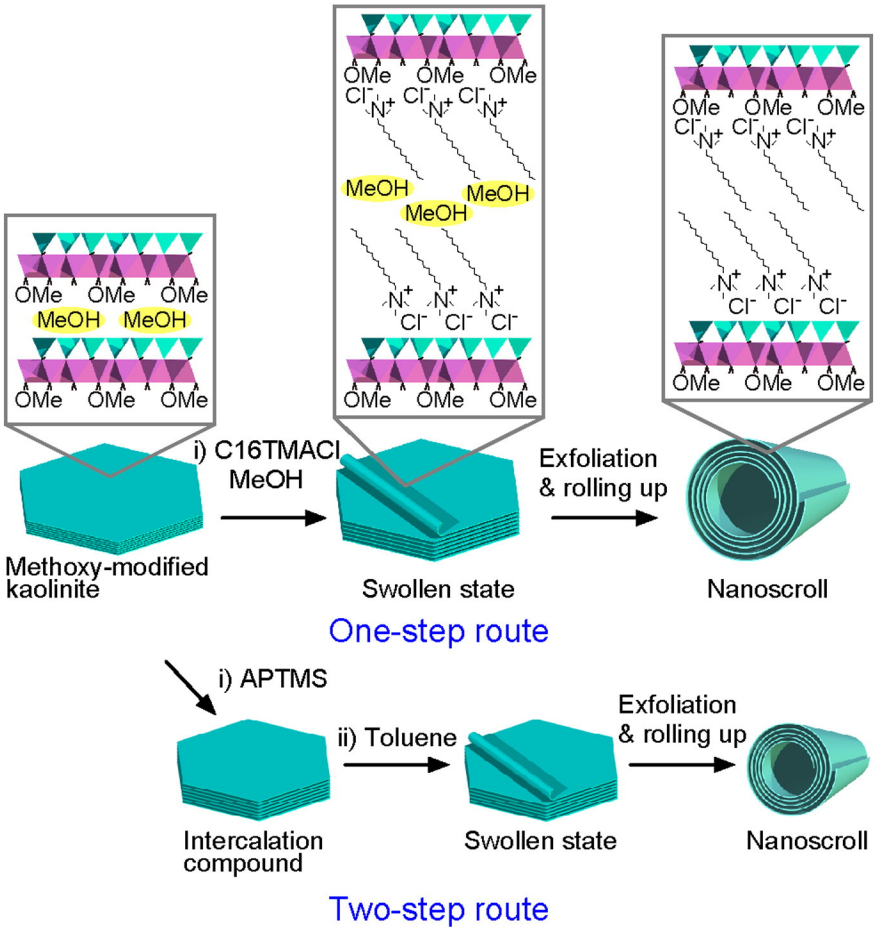

Fig. 3. Schematic representatives of the exfoliation and transformation of methoxy–modified Kaol into nanotubes by the one- and two-step routes. Reprinted with permission from Kuroda et al. (2011). Copyright (2015) American Chemical Society.

low tubular quality, characteristic of high irregularity in diameter, wall thickness, and morphology (Yuan et al., 2008). Furthermore, tubular Hal with different wall-thicknesses also have different spiral structures, for example, the thick-walled Hal presented by a Power spiral and the thin-walled Hal presented a Logarithmic spiral (Mitra, 2013).

Hal possesses a relatively high specific surface area (*SSA*) and a total pore volume (V_{pore}) that is much higher than that of platy Kaol but usually lower than that of montmorillonite. This should be ascribed to the abundant pores in the structure of Hal. There are three types of pores in Hal: i) the newly formed mesopores in the tube-wall during dehydration, resulting from the originally tightly connected rolled layers in fully hydrated Hal separating because of dehydration and thus creating slit-shaped longitudinal pores with a width of several nanometers (Kohyama et al., 1978; Churchman et al., 1995); ii) the inherent mesoscopic or even macroscopic lumens (the inner cavity of the tubular Hal particle); and iii) the voids formed among particles in agglomerates (50–100 nm) (Liu et al., 2007; Forsgren et al., 2010). The porosity values of Hal from different deposits are also significantly different (Table 1) because of the different morphologies and the presence of various associated minerals (Joussein et al., 2005; Pasbakhsh et al., 2013).

3.3. Structural and morphological changes under thermal treatment

The behavior of Hal under heating has been postulated to be analogous to that of Kaol because of its structural and chemical similarity with Kaol. Numerous studies on the calcination of Kaol have been conducted in the past half-century, since Brindley and Nakahira (1959) pioneered the study of the Kaol-to-mullite reaction sequence.

Table 1
Morphological and textural characteristics of Hal samples sourced from different deposits.

Sample	Deposit	*L* (nm)	*D* (nm)	*d* (nm)	*T* (nm)	*R*	*SSA* (m^2/g)	V_{pore} (cm^3/g)
CLA[a]	Camel Lake, South Australia	800–900	40–64	17–23	15–21	16	49.5	0.25
CLA[b]	Camel Lake, 63 km of Maralinga, South Australia	100–1500	20–70	10–50	5–30	17	74.7	0.17
PATCH[a]	Kalgoorlie, Western Australia	3500–4500	33–39	17–21	5–11	1100	40.3	0.08
PATCH[b]	Siberia, 85 km NW of Kalgoorlie, Western Australia	200–5000	40–55	12–22	8–20	50	81.6	0.18
HG[a]	Northland, New Zealand	100–300	19–40	8–26	8–18	6	23.2	0.13
MB[b]	Matauri Bay, Northland, New Zealand	100–3000	50–200	15–70	20–100	12	22.1	0.06
JA[b]	Jarrahdale, Western Australia	50–1000	30–80	10–30	10–25	10	44.6	0.12
DG[b]	Dragon Mine, Utah, USA	50–1500	20–150	5–30	5–50	9	57.3	0.12
TP[b]	Bay of Plenty, New Zealand	100–1500	30–50	10–20	8–12	–	33.3	0.09

L, the length of Hal particle. *D*, the external diameter. *d*, the internal diameter. *R*, the aspect ratio, where, $R = L/D$. *T*, the wall thickness. *SSA*, specific surface area. V_{pore}, total pore volume.
[a] Yuan et al., 2008.
[b] Pasbakhsh et al., 2013.

The thermal dehydroxylation and transformation of Kaol is one of the most thoroughly investigated reactions (Rocha and Klinowski, 1990) because of its importance in ceramic processing. The intermediate states and the equilibrium end point of the Kaol–mullite reaction have been well defined using various methods, including magic angle spinning nuclear magnetic resonance (MAS NMR) (Brown et al., 1985; MacKenzie et al., 1985; Rocha and Klinowski, 1990; Massiot et al., 1995), transmission electron microscopy (TEM) (Bergaya et al., 1996; Lee et al., 1999), infrared spectroscopy (Vassallo et al., 1992; Frost and Vassallo, 1996), electron paramagnetic resonance (Djemai et al., 2001), X-ray diffraction (XRD), and thermal analysis (Dion et al., 1998; Kristóf et al., 1998).

Much less attention has been paid to the thermal transformation of Hal than to that of Kaol. Smith et al. (1993) conducted a comprehensive study to investigate the structural changes upon the thermal decomposition of tubular Hal under progressive heating up to 1400 °C using a combination of ^{29}Si and ^{27}Al solid state NMR, XRD, and TEM. These authors demonstrated that the thermal transformation of Hal is largely similar to that of Kaol. In principle, it can be concluded from the above mentioned studies that the reaction scheme for the calcination of Kaol or Hal initially involves dehydroxylation between 600 °C and 850 °C, where most of the hydroxyl groups are removed, leading to the reduced coordination of the originally octahedral aluminum. Moreover, a large exothermic event at approximately 980–1000 °C, believed to be triggered by the removal of the last hydroxyls, is due to the formation of a distinct alumina-rich phase. Further heating to 1400 °C results in the final equilibrium products, namely a 3:2 mullite ($3A1_2O_3 \cdot 2SiO_2$) and cristobalite. In particular, Smith et al. (1993) presented clear evidence that the major exotherm of Hal at approximately 1000 °C was mainly associated with the formation of γ-Al_2O_3 on a very fine scale (<5 nm). This result could be considered as a convincing answer to the debate as to whether the alumina-rich phase formed in this event is a spinel-like γ-Al_2O_3 or an alumina-rich mullite (Okada et al., 1986; Sonuparlak et al., 1987).

Yuan et al. (2012a) further investigated the morphological and textural characteristics as well as the surface reactivity of calcined tubular Hal. This study is based on the assumption that when Hal is calcined, significant changes in porosity arise because of the one-dimensional porous structure of tubular Hal, in contrast with the plate-like non-porous nature of Kaol. A high purity tubular Hal sample was used in the mentioned work to avoid the effects of impurities on the interpretation of the spectroscopic characterization and to increase the reliability of the obtained results. This study provided a detailed description of the morphological changes such as the closing of the nanotube at one or both ends for some Hal at approximately 1100 °C. Moreover, a direct HRTEM observation (Fig. 4) showed the formation of nanocrystalline γ-Al_2O_3 at approximately 1000–1100 °C, evidenced by SAED and by the high-resolution lattice image of nanocrystalline γ-Al_2O_3 domains with a width and length of approximately 5 nm and 5–15 nm, respectively.

Another interesting observation in the same work (Yuan et al, 2012a) is that the rough tubular morphology and the mesoporosity of Hal remained largely intact as long as the heating temperature was lower than 900 °C. The values of the *SSA* and V_{pore} of Hal calcined at 900 °C are even 10% larger than those of the dried initial Hal, which might be attributed to the formation of micropores during surface breakage, resulting from either structural rearrangement or transformation. The high thermal persistence of the tubular structure of Hal should be meaningful for the design of novel Hal-based nanocomposite or ceramic materials. For example, a high thermal stability can be postulated for nanosized products of Hal-metal oxide reactions although they have rarely been investigated (Antill, 2003). Moreover, the curving and closing of the ends of the tubes may provide a solution for the encapsulation of materials within guest-loaded Hal-derived nanotubes for controlled-release purposes. This encapsulation for release control has been attempted using several methods (Lvov et al., 2008; Abdullayev and Lvov, 2011; Yuan et al., 2012b). It is noteworthy that small variations in the threshold values of the critical thermal stability temperature, *i.e.*, the highest temperature point at which the porosity of Hal remains almost intact, are very likely to exist among natural Hal specimens of different sources (Ouyang et al., 2014). This may be due to the diversity in morphological parameters (length, internal/external diameter, and thickness of tube) of the Hal nanotubes (Pasbakhsh et al., 2013) and to the presence of impurity minerals possibly affecting the behavior of Hal upon heating.

3.4. Structural and morphological changes under acid or alkaline treatment

Acid or alkaline treatment is one of the most commonly used methods for the processing of industrial minerals. Theoretically, both acid and alkaline treatment could potentially damage the structure of Hal, since dealumination and desilication would occur under strong acid and alkaline conditions, respectively. However, Joo et al. (2013) demonstrated that the chemical structure of Hal was maintained after a relatively mild acid or alkaline treatment, *i.e.*, in solutions with pH values from 2 to 11; instead, the pH of a solution can substantially influence the overall charge of Hal, indicated by changes in ξ-potential. These authors found that the ξ-potentials were −3.5, −32.4, and −44.8 mV at solution pH = 2, 7, and 11, respectively; moreover, an apparent correlation exists between the pH of the solutions, the dispersion behavior of Hal in the solutions, and the porosity of dry Hal powders. It is noteworthy that the dry Hal powders were obtained after freeze-drying, which was used to achieve a maximum preservation of the aggregation state of the Hal particles. In addition, at pH = 2 the Hal dispersion was unstable leading to aggregation of the Hal nanotubes which formed large bundles. But at higher pH (>8), the agglomeration and precipitation of Hal particles did not occur due to van der Waals interaction between the particles and particularly, at pH = 11, the degree of Hal dispersion was the highest among the tested pH (Joo et al., 2013). These phenomena significantly affect the pore diameter, pore surface area, and pore volume of Hal. As schematically illustrated in Fig. 5, in alkaline solution, Hal was well dispersed and each end was separated from other Hal nanotubes, allowing the opening access of

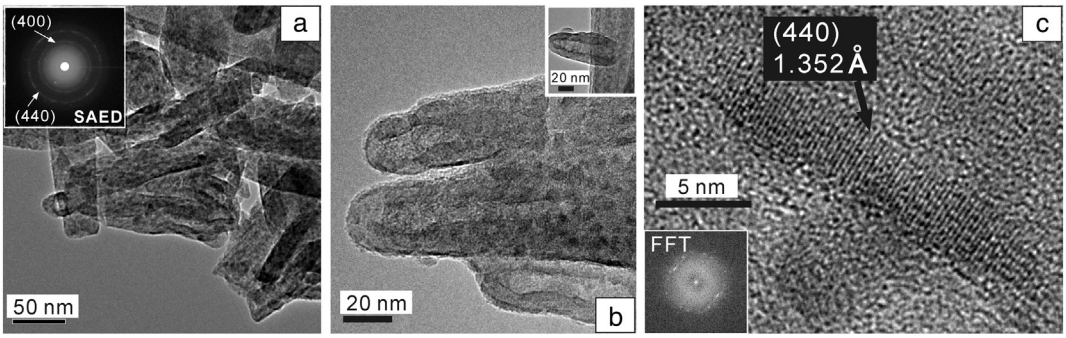

Fig. 4. TEM images of calcined Hal. Adapted from Yuan et al. (2012a) with permission.

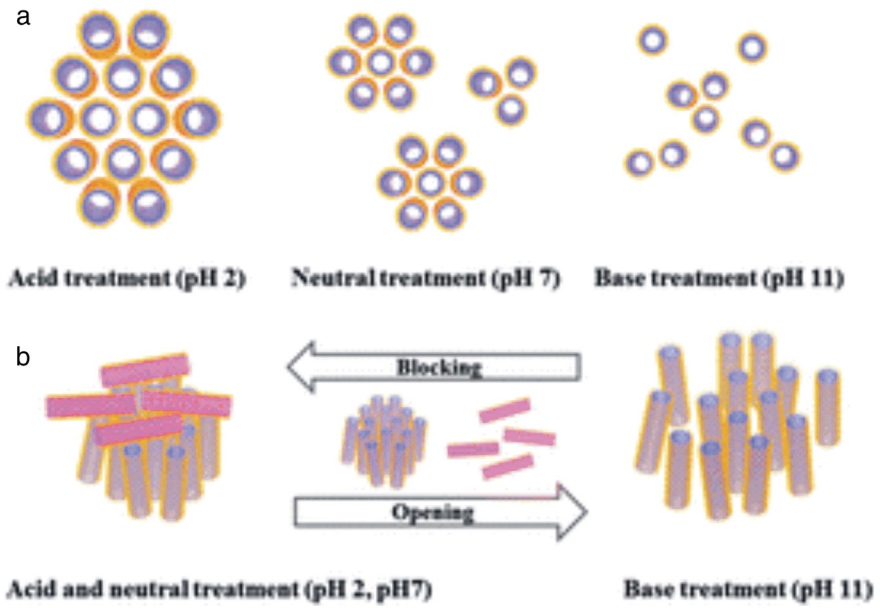

Fig. 5. Aggregation and dispersion behaviors of Hal nanotubes in solution with different pH. Reprinted from Joo et al. (2013) with permission.

the Hal inner pores; whereas, in acidic solution, Hal bundles were located adjacent to the ends of other Hal nanotubes, resulting in a blocking of the Hal inner pores. This effect was verified by porosity characterizations using nitrogen adsorption desorption isotherms of the dry Hal products. The changes in pore volume, pore area, and pore size are in good agreement with the aforedescribed opening and blocking of Hal nanotubes based on aggregation and dispersion upon mild alkaline, acid, or neutral treatment.

In highly concentrated acid and/or alkaline solutions, the structure of Hal undergoes significant changes. White et al. (2012) conducted a detailed study of the long-term stability of natural Hal under strong acidic and alkaline conditions. These authors showed that the Hal nanotubes were corroded in quite different ways in 1 M solutions of strong acidity and/or basicity. As schematically presented in Fig. 6, in the acid-assisted corrosion of Hal, the inner AlO_6 octahedral surface is first attacked by the acid, resulting in the release of Al^{3+} in the solution after an induction period. Further dissolution continues predominantly on the inner surface of the lumen, leading to the release of Si^{4+}, which rapidly reaches a saturated concentration and gradually precipitates in the form of amorphous SiO_2 in the lumen of the nanotubes. The formation of amorphous SiO_2 as small spheroidal nanoparticles approximately 10 nm in diameter in the lumen was observed *via* TEM. The decomposition of Hal in 1 M NaOH solution is also initiated on the inner surface of the nanotubes, leading to the release of Si^{4+} in the solution, whose solubility in alkaline environments is greater than that of Al^{3+}. Unlike corrosion in an acid environment, the crystallization of saturated Al^{3+} occurs predominantly outside the nanotubes in the form of flat $Al(OH)_3$ nanosheets, which is possibly a result of crystallization induced by the partially dissolved fragments of the Hal walls composed of AlO_6 octahedrons.

The strong acid and alkaline treatments led to an increase in both *SSA* and V_{pore} compared with the original Hal (24.3 m^2/g and 0.09 cm^3/g, respectively). The treatment with both HCl and H_2SO_4 resulted in an almost linear increase in *SSA* and V_{pore} with time, whereas the initial growth was followed by steady state values after 28 days in the case of NaOH. The treatment with 1 M H_2SO_4 resulted in the largest

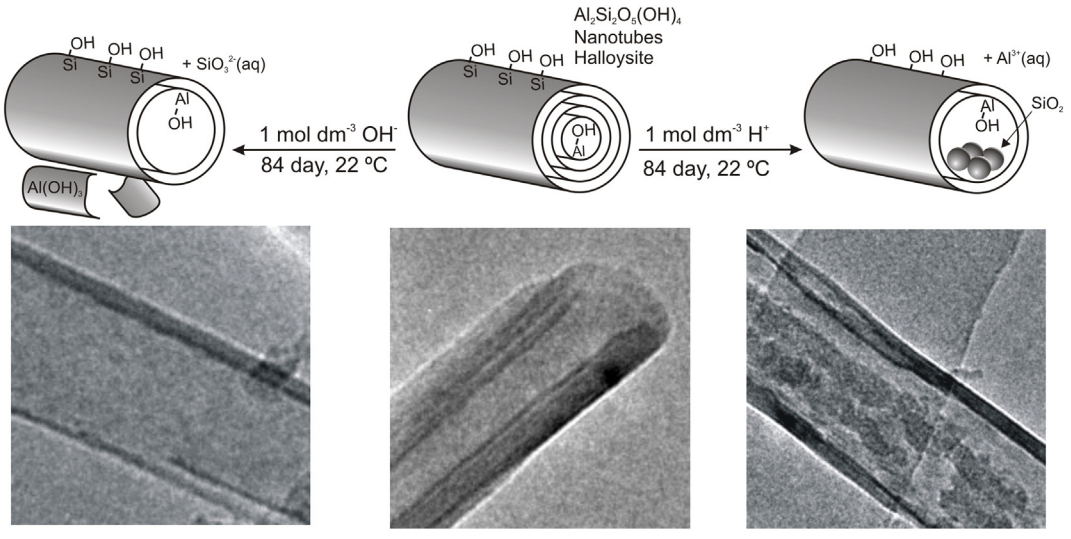

Fig. 6. Scheme of transformation of Hal in strong acid and alkaline solutions. Reprinted from White et al. (2012) with permission.

increase in *SSA* and V_{pore} (approximately threefold after 28 days and fourfold after 84 days). Moreover, the acid and base treatments also substantially altered the wall thickness of the Hal nanotube. After 1 M H_2SO_4 treatment for 84 days, the average external diameter of the nanotubes remained unchanged, whereas the average internal diameter increased from 15 nm for the original Hal to 22.9 nm and the average wall thickness decreased from 15 nm to 10.3 nm. After treatment with 1 M NaOH for 84 days, the average internal diameter increased to 22.8 nm, the average wall thickness decreased to 11.4 nm, and the average external diameter remained unchanged. A similar increase in *SSA* and V_{pore} with treatment time, as well as the destruction of the AlO_6 octahedral layer structures and the formation of amorphous silica nanoparticles were observed by Zhang et al. (2012a) and Abdullayev et al. (2012). However, to test the stability of Hal over a relatively short time (<60 h), an acid was used with a higher concentration, *i.e.* 2 M or even 3 M H_2SO_4 than that used in the above-mentioned study (White et al., 2012). A ^{29}Si solid-state MAS NMR investigation evaluating the structural changes of the Hal at the atomic scale showed that the hydrolysis of two Si–O–Al and two Al–OH–Al bonds occurred during the release of single Al^{3+} ions. Two newly formed broad chemical shifts centered at approximately −100 ppm and −109 ppm were assigned to the Q^3-type silicon sites with one second nearest-neighbor aluminum $Si(OSi)_3$–(O^+AlH) and to the Q^4-type $Si(OSi)_4$ sites of amorphous silica-like regions in the dealuminated Hal products, respectively (Abdullayev et al., 2012). ^{27}Al solid-state MAS NMR spectra showed that the environment of atoms of alumina was identical to that of the original Al–OH–Al layers of Hal but that significant alterations occurred at a very high level of dealumination (above 90%).

The structural changes induced by acid treatment are expected to change the mechanical properties of Hal. Abdullayev et al. (2012) estimated that the Hal bending stiffness and tensile strength were reduced due to the decrease in wall thickness resulting from the acid treatment. However, a more accurate evaluation of the effects of the acid treatment on the change in the mechanical properties of Hal could be achieved only by directly measuring the Young's modulus of Hal using proposed methods based on TEM (Lu et al., 2010) and atomic force microscopy (AFM) (Lecouvet et al., 2013a). The aforementioned studies revealed the stability of Hal in acid or alkaline solutions, which is meaningful for the understanding of the behavior of Hal in natural environments, *e.g.*, how its surface reactivity is possibly modified in acidic soils. In addition, these results are useful for applications where Hal interacts with acids or bases. The increased *SSA* and V_{pore} of the resulting nanotubes, without any significant shape alteration after the acid or alkaline treatment, could be desirable for applications of modified Hal; for example, the acid-modified Hal has been proven to be an effective adsorbent for methylene blue (Zhang et al., 2012b). In concentrated NaOH solutions, the thinning of the tube walls of Hal without the creation of SiO_2 nanoparticles inside the tubes might have uses in applications where a larger internal diameter is required, such as the encapsulation of large proteins or DNA molecules (White et al., 2012). Moreover, the enlargement of the Hal lumen i) increased the loading efficiency of benzotriazole (a corrosion inhibitor) by 4 times, which is comparable to the conventional polymeric microencapsulation technique, and ii) allowed increasing diameter of the silver nanorods to be encapsulated in the acid-modified Hal (Abdullayev et al., 2012).

4. Physico-chemical properties and surface chemical modifications of halloysite (Hal)

4.1. Mechanical properties of Hal nanotube

The clay mineral layer has by itself several excellent mechanical properties. For example, the in-plane elasticity of a single layer of montmorillonite is as high as 270 GPa, according to a Monte Carlo simulation (Manevitch and Rutledge, 2004). Theoretically, the mechanical properties of Hal are also important for its practical applications. As Hal is used as inorganic filler in CPN, its mechanical properties, combined with other important factors such as loading amount and aspect ratio of the filler, dispersion extent, and compatibility between filler and organic substrate, strongly influences the mechanical properties of the final CPN product (Liu et al., 2014). Until now, there were only few studies investigating the mechanical property of a single Hal nanotube because it is difficult to directly assess the mechanical property of nanosized Hal. Guimaraes et al. (2010) calculated the mechanical properties of *zigzag* and *armchair* single-walled Hal nanotubes using the self-consistent charge density-functional tight-binding method, and they found that the Young's modulus for the *zigzag* and *armchair* Hal was in the range of 230–300 GPa and 300–340 GPa, respectively. This discrepancy arises from the different diameters of the *zigzag* (15–36 Å) and of the *armchair* (21–46 Å) Hal.

Lu et al. (2010) directly measured the Young's modulus of a single Hal nanotube by using a TEM with a bending stage. The obtained experimental Young's modulus (130 ± 24 GP) is lower than the calculated value for the single-walled Hal (230–340 GPa) because Hal is composed of multi-walled nanotube rolled by 15–20 aluminosilicate layers (Lvov et al., 2008) including structural defects. Moreover, the Young's modulus of Hal decreased with the increase in wall diameter because Hal with a greater diameter has a higher density of structural defects. In addition, these authors also found that the Hal nanotubes are surprisingly flexible and could be bent to almost 90° without fracture.

Lecouvet et al. (2013a) measured the elastic modulus of Hal nanotubes using AFM with three-point bending tests. When the external diameter of Hal ranged between 50 and 160 nm, the average elastic modulus was 140 GPa. This result is in agreement with the observation made by Lu et al. (2010). When the external diameter of Hal was less than 50 nm, the elastic modulus suddenly increased to 460 GPa. This value is even greater than the calculated elastic modulus of single-walled Hal nanotube (Guimaraes et al., 2010) and that of a single layer of montmorillonite (Manevitch and Rutledge, 2004). This unexpected steep jump in elastic modulus for the Hal nanotubes with small diameters is principally due to the surface tension effect and the absence of structural defects.

4.2. Interlayer water molecules and dehydration behaviour

The interlayer water molecules in Hal-(10 Å) can be classified into two types: i) “hole water”, embedded into the ditrigonal cavities in the basal oxygen plane with two main different orientations and forming hydrogen bonds with the basal oxygen; and ii) “associated water”, located at a different levels in the interlayer space, with an ice-like configuration and a high degree of mobility and forming hydrogen bonds with each other and/or with inner-surface hydroxyls (Hendricks and Jefferson, 1938; Lipsicas et al., 1985; Smirnov and Bougeard, 1999). Because the more stable “hole water” is lost more slowly than the “associated water”, Hal occurs in an intermediate state between a fully hydrated and fully dehydrated form, similar to the intermediate states for Kaol: Kaol-(8.6 Å) and Kaol-(7.9 Å) reported by Giese (1988). The two intermediate states of Hal-(8.6 Å) and Hal-(7.9 Å) were directly observed on the SAED pattern of hydrated Hal obtained *via* TEM with an environmental cell (Kohyama et al., 1978).

Generally, the interlayer water molecules, weakly held by hydrogen bonds, are readily and irreversibly lost. This dehydration of Hal-(10 Å) depends on the drying history, relative humidity (RH), and sample origin (Hughes et al., 1966; Joussein et al., 2005). For instance, Hal-(10 Å) undergoes dehydration at 40 °C at 40% RH but at 65 °C for 100% RH (Kohyama et al., 1978). The dehydration of Hal-(10 Å) by heating at 100–350 °C induced the basal spacing to decline to 7.2 Å, which is slightly larger than the basal spacing of Kaol (7.14 Å). This is accomplished only under the condition that 15 layers of Kaol contain one layer of water (Brindley and Robinson, 1946). The complete removal of the interlayer water molecules is achieved upon heating at 400 °C without dehydroxylation (Brindley et al., 1949).

Dehydration can have different effects on spheroidal and tubular Hal. For spheroidal Hal, dehydration induced a reduction in particle diameter (Joussein et al., 2005). For tubular Hal, dehydration unfolded the layer of Hal showing a 10–20% increase in diameter. This unfolding process also generated the splitting of the tightly connected layers, forming slit-shaped nanopores (Kohyama et al., 1978). In addition, dehydration could impact the structure of Hal. High-resolution TEM observation showed that dehydrated Hal consists of helically rolled parallel cylinders containing spiral cell structures, whereas hydrated Hal has a more doughnut-like structure (Ece and Schroeder, 2007).

The presence of interlayer water molecules has a great influence on the reactivity of Hal. The interlayer water is favorable for the intercalation of organic compounds; however, the dehydrated Hal is only partly intercalated with formamide and ethylene glycol (Joussein et al., 2005). Moreover, the interlayer water could significantly influence the grafting of organosilanes on Hal by affecting their hydrolysis (Yuan et al., 2008; Tan et al., 2013).

4.3. Surface modification of Hal

Surface modification refers to the introduction of functional groups onto the surface of a host material, which can be achieved by either physical modifications (wrapping the modifier onto the host by van der Waals forces, hydrogen bonding, and electrostatic attraction) or chemical modifications (by covalently attaching the modifier to the host). The physical properties (solubility, dispersion, hydrophilicity/hydrophobicity, *etc.*) and the chemical properties (reactivity, biotoxicity, *etc.*) of the host can be carefully tailored for a specific surface-modification, and will consequently promote the performance of the host when used in some applications. In the case of Hal, multiple surfaces (the external surface, the interlayer surface, and the internal lumen surface) could potentially be modified. The external surface is composed of siloxane (Si–O–Si) groups and of a small number of aluminol (Al–OH) and silanol (Si–OH) groups exposed on the edges and surface defects of the Hal (Yuan et al., 2008). The interlayer surface and the internal lumen surface consist of a gibbsite-like array of aluminol (Al–OH) groups. The chemical difference between the external and internal surfaces of Hal results in a positive zeta potential for the internal surface and a negative zeta potential for the external surface over a pH range of 2.5 to 8.5 (Veerabadran et al., 2007). In addition, Hal is highly hydrophilic, with the water contact angle for Hal being as low as 10 ± 3° (Abdullayev et al., 2009). When Hal was used as filler in polymers, as adsorbent for pollutants, and as carrier for active guest molecules, Hal showed only a weak affinity (ion exchange, hydrogen bonding, and van der Waals forces) for the guest. To improve the performance of Hal in the abovementioned areas, a surface modification of Hal, normally site-specific and sometimes selective, is highly desirable.

4.3.1. Modification of the external surface

The external siloxane surface of Hal has a low chemical activity and is unavailable for grafting by organic compounds. However, due to the negative surface potential in a wide pH range, it is possible to modify the external surface property of Hal by adsorbing some specific cations. Lvov et al. (2002) adsorbed poly(ethyleneimine) (PEI) on the surface of Hal to form a monolayer with a thickness of 54 nm and then alternately adsorbed Hal and PEI to generate thin films with a thickness of 720 nm (approximately 14 sets of Hal-PEI monolayers). Due to the loosely packed Hal in the Hal-PEI monolayer, the thin film consists of a network with 50% empty space, which could be used as loading space for the subsequent controlled release of guest molecules. Veerabadran et al. (2009) used layer-by-layer (LBL) assembly to form organized shells on the pre-loaded Hal for the controlled release of dexamethasone. As illustrated in Fig. 7, the organized shells were synthesized by alternately adsorbing polycations (poly(allylamine) hydrochloride; PAH; PEI; chitosan) and polyanions (sodium poly(styrene sulfonate): PSS; poly(acrylic acid): PAA; gelatin) on the external surface of Hal. The sequential polycation/polyanion assembly changed the surface potential of Hal from a positive value to a negative value. The organized shell could significantly decrease the diffusion of dexamethasone from the lumen of Hal.

Shamsi and Geckeler (2008) developed an interesting method to modify the external surface of Hal by wrapping DNA on the surface of a Hal nanotube through a mechanochemical reaction in the solid state. The DNA-wrapped Hal is obtained by simply milling DNA and Hal. After the milling, the Hal nanotubes were cut into shorter lengths but the DNA remained intact and completely covered the surface of the Hal. This modification afforded Hal with a high aqueous solubility and revealed some potential biomedical applications for Hal nanotubes. Chang et al. (2011) wrapped amylose on the surface of Hal to improve their biocompatibility. The obtained Hal amylose nanocomposite has a good dispersion in a DMSO/H_2O solution.

In addition to modifications on the external siloxane surface of Hal, Yuan et al. (2012a) demonstrated that the original siloxane groups at the external surface could also partially or entirely replaced by hydroxyl groups after calcination at 600–900 °C, and that the newly formed surface hydroxyl groups of the calcined Hal were available for covalent grafting with organosilanes (3-aminopropyltriethoxysilane: APTES). The formation of the hydroxyl groups occurred before the breakdown of the tubular structure and accompanied the disconnection and further disordering of the silica and alumina originally present in the tetrahedral and octahedral sheets. Based on this finding, novel applications of calcined Hal could be postulated. For example, the hydroxyl groups formed could act as new active sites for attracting and fixing functional guests because of their availability for ion exchange and silylation reactions. Moreover, the organo-modification of the external tube

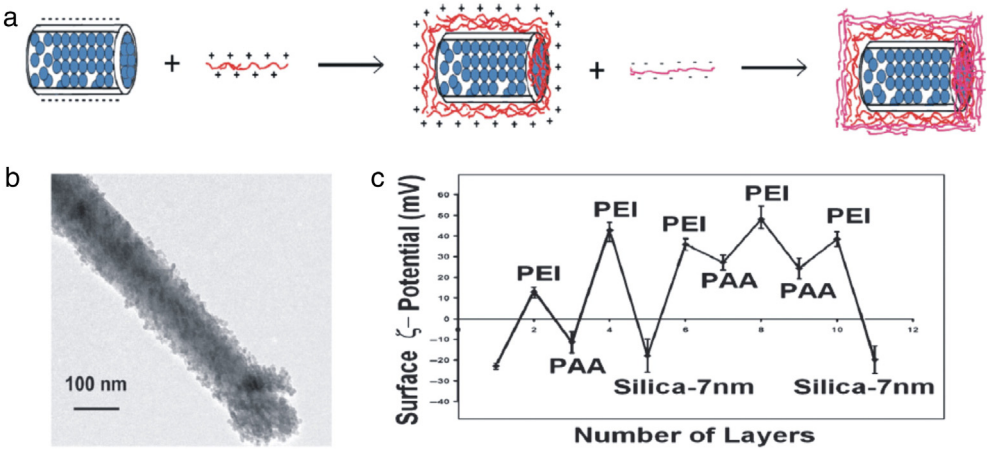

Fig. 7. LBL assemble of Hal. Reprinted from Abdullayev and Lvov (2011) with permission.

surface of calcined Hal promises to be a particularly versatile yet site-specific approach to improve the affinity between the calcined Hal and the polymer substrate in Hal–polymer nanocomposites. To our knowledge, this last approach has not yet been explored. These external tube surface-based potential applications may significantly extend the utility of current lumen-based applications of Hal. These applications are summarized in detail in the following sections.

4.3.2. Selective modification of the internal lumen surface

The Al–OH groups on the internal lumen surface of Hal have a high chemical activity toward many organic compounds such as organosilanes. The surface modification of Hal could be accomplished through the covalent grafting of functional groups on the internal lumen surface. Yuan et al. (2008) investigated the modification of Hal by the grafting of 3-aminopropyltriethoxysilane (APTES) on the lumen surface; a layer of aminopropyl groups was introduced and implanted through the formation of covalent Al–O–C bonds by the condensation of the Al–OH groups of Hal and the hydroxyl groups of the hydrolyzed APTES. As shown in Fig. 8a, the general mechanism of APTES grafting on Hal can be described as follows: i) condensation occurs between the hydroxyl groups of the hydrolyzed APTES and those of Hal, including the Al–OH at the internal lumen surface and the Al–OH and Si–OH at the edges or surface defects, resulting in the grafting of APTES mainly in the lumen of Hal; and ii) some of the hydrolyzed APTES condenses with each other to form oligomers which grafted by covalent and/or hydrogen bonds with the already grafted APTES, forming a cross-linked network in the lumen.

The grafting of APTES could promote the functionality but sacrifice the porosity of Hal (Yuan et al., 2008). The extent of the APTES grafting is determined by i) the origin of the Hal. For instance, Hal with a high *SSA* have a higher content of grafted APTES than Hal with a low *SSA* because Hal with higher *SSA* have a higher density of hydroxyl groups on the surface allowing more grafted APTES. ii) by its pretreatment (heating, evacuation, *etc.*). For instance, a thermal pretreatment at

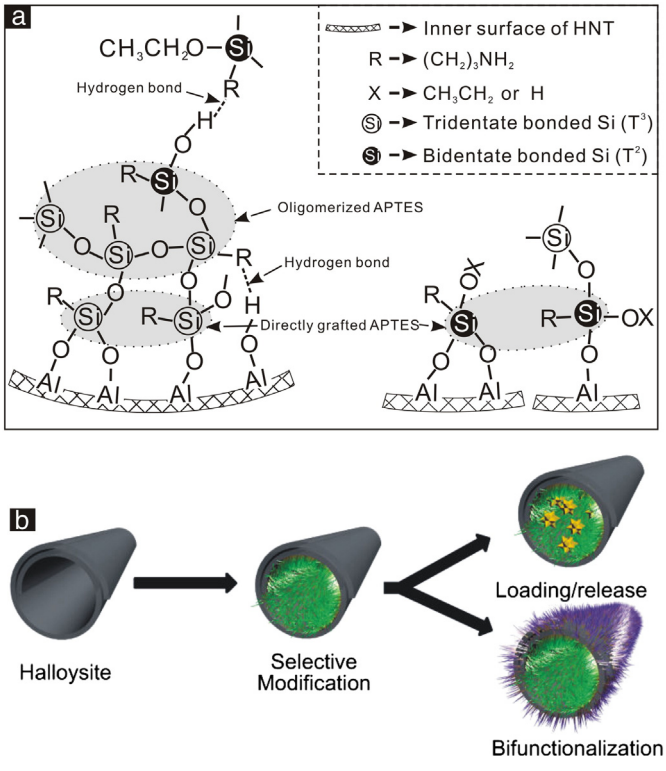

Fig. 8. Schematic representation of the grafting of (a) APTES and (b) octadecylphosphonic acid on Hal. Reprinted with permission from Yuan et al. (2008) and Yah et al. (2012a). Copyright (2015) American Chemical Society.

400 °C reduces the water content and leads to a restriction of the APTES oligomerization and the subsequent formation of the cross-linked network in the lumen, which consequently preserved the lumen space. Also the removal of air from the lumen by evacuation treatment is useful for enhancing the loading of APTES, and hence for increasing the extent of grafting or oligomerization. Therefore, the pretreatment conditions must be carefully tailored to optimize the organosilane-grafting of Hal.

The grafting of APTES introduced, on the surface of Hal, amino groups which have a high chemical activity and can react with other functional groups to further modify the surface of the Hal. Joo et al. (2012) synthesized a carboxylic acid functionalized Hal (Hal–COOH) from amino-functionalized Hal (Hal–NH_2) through the reaction between the succinic anhydride and Hal–NH_2 in dimethyl formamide. The obtained Hal–COOH formed aggregates in neutral solution because of the hydrogen bonds between the carboxyl groups of Hal–COOH; however, Hal–COOH was well dispersed in acidic solution, and even monodispersed in basic solution, which can be rationalized as resulting from the decrease in hydrogen bonding in acidic solutions, and the repulsive forces generated between the carboxylate anions in basic solution. The carboxylic acid functionalized Hal with excellent dispersion is of great potential application in CPN, catalysts, drug delivery systems, and cosmetics.

In addition to the internal lumen surface modification of Hal by grafting of organosilanes, other organic compounds for the selective modification of the internal lumen surface were explored. Yah et al. (2012a) found that octadecylphosphonic acid could selectively bind onto the lumen of Hal through bidentate and tridentate P–O–Al linkages (Fig. 8b). This modification afforded Hal with a hydrophobic lumen and a hydrophilic external surface. Compared with unmodified Hal, the modified Hal has a higher adsorption capacity for hydrophobic ferrocene because the hydrophobic tubular core acts like a sponge to embed ferrocene into its alkyl chains but has a lower adsorption capacity for hydrophilic ferrocenecarboxylic acid because of the favorable hydrogen bonding in the unmodified Hal. In addition, the Hal already modified by organophosphonic acid on the internal lumen surface could be further grafted by N-(2-aminoethyl)-3-aminopropyltrimethoxysilane on the external surface, thus achieving a bifunctionalization of the Hal. This bifunctionalized Hal might enable different potential applications from water purification to drug immobilization and controlled release. Furthermore, Yah et al. (2012b) immobilized 2-bromo-N-[2-(3,4-dihydroxyphenyl)ethyl]-isobutyryl amide (Dopa), a dopamine derivative, onto the internal lumen surface of Hal. Theoretically, Dopa binds to both the silica-like external surface and the alumina-like internal lumen surface of Hal through silica–catechol bonds and alumina–catechol bonds, respectively. However, the weak silica–catechol bonds could be readily removed by sonication and tetrahydrofuran–water solution rinses. Therefore, the more stable alumina–catechol bonds could be maintained, allowing the selective modification of the Al–OH groups on the lumen of Hal.

4.3.3. Modification of the interlayer surface

Although the surface hydroxyl groups of the internal lumen surfaces, edges, and external surfaces of Hal could be grafted by organic compounds (Yuan et al., 2008; Yah et al., 2012a,b), the interlayer inner-surface Al–OH groups were unavailable for grafting because they were blocked by the strong hydrogen bonds between adjacent layers. For Kaol, the grafting of APTES onto the interlayer inner-surface hydroxyl groups could be achieved only under severe conditions (*e.g.*, pre-intercalation of dimethyl sulfoxide (DMSO), pure APTES liquid, high temperatures, and N_2 atmosphere) (Tonlé et al., 2007; Yang et al., 2012). The reaction temperature had a significant influence on the grafting of APTES onto the interlayer inner-surface hydroxyl groups of Kaol. In the case of a high reaction temperature (220 °C), the APTES arranged in a cross-linked monolayer in the interlayer space, with a basal spacing of 1.00 nm; in the case of low reaction temperatures

(175, 185, and 195 °C), the APTES acted as a pseudo-bilayer arrangement in the interlayer space, with a basal spacing of 1.73–1.89 nm (Fig. 9). However, this interlayer surface modification by APTES has not yet been achieved in the case of Hal under the same conditions (Yang et al., 2012).

Regardless of the strong hydrogen bonds between adjacent layers of Kaol and Hal, some organic molecules, such as DMSO and methyl formamide, could directly intercalate into the interlayer space of Kaol and Hal (Joussein et al., 2005). The organic molecules that cannot be directly intercalated into the interlayer space, such as methanol, diethanolamine, triethanolamine, tris(hydroxymethyl)aminomethane, pyridine–carboxylic acids, APTES, 1-(2-Hydroxyethyl)-3-methylimidazolium, and terbium pyridine–picolinate, could be intercalated by replacing the pre-intercalated organic precursors and reacting with the interlayer inner-surface Al–OH groups to accomplish the modification of the interlayer space of Kaol and Hal (Tunney and Detellier, 1996; Letaief and Detellier, 2007; Tonlé et al., 2007, 2009; de Faria et al., 2009, 2010, 2011; Yang et al., 2012; Matusik and Wścisło, 2014). For example, the grafting of methoxy groups on the interlayer inner-surface Al–OH groups of Kaol was first proposed by Tunney and Detellier (1996). The grafting mechanism is as follows: methanol molecules are intercalated into the interlayer space of Kaol by replacing the pre-intercalated DMSO or methyl formamide and then one methanol molecule is condensed with one interlayer inner-surface Al–OH group to form Al–O–C bonds and one H_2O molecule. Part of the grafted methoxy groups was keyed into the $(SiO)_6$ macro-ring of the adjacent silicate sheet. The grafting of the methoxy groups induced an increase in basal spacing of 0.82–0.86 nm, depending on the number of interlayer water molecules generated by the condensation between methanol molecules and Al–OH groups.

The interlayer space of the methoxy-modified Kaol has been used as host for guest molecules, such as ε-caprolactam (Komori et al., 1999a), poly(vinylpyrrolidone) (Komori et al., 1999b), alkylamines (Komori et al., 1999c), *p*-nitroaniline (Kuroda et al., 1999; Takenawa et al., 2001), nylon 6 (Matsumura et al., 2001), some quaternary ammonium salts (Kuroda et al., 2011), 5-fluorouracil (Tan et al., 2014a), and amitrole (Tan et al., 2015). In addition, the interlayer space of the methoxy-modified Hal is also available for the loading of guest molecules, such as the anticancer drug 5-fluorouracil and the herbicide amitrole. The methoxy-modification introduced a plane of methoxy groups into the interlayer space of Kaol/Hal weakening the original hydrogen bonds between adjacent layers. This interlayer space became available for further intercalation. The intercalated guest exhibited a high level of loading and a controlled release because of the development of this additional loading space and the significant diffusional restriction by the lamellar structure (see more details in Section 5.2).

5. Hal-based advanced materials and their applications

The abundant nanosized tubular Hal has excellent mechanical property and good biocompatibility. These advantages allowed a variety of potential applications in many fields, *e.g.*, as filler in polymers, carrier for the loading and controlled release of guest molecules, adsorbent for pollution remediation, and a nanoreactor/nanotemplate for the synthesis of functional materials.

5.1. Hal–polymer nanocomposites

Hal is expected to be a promising filler for Hal–polymer nanocomposites due to its aforedescribed high *SSA*, high aspect ratio, good dispersion, and excellent mechanical properties. Many studies investigated the effect of Hal as filler on the mechanical properties, thermal stability, and flame retardancy of polymers (Du et al., 2010a; Liu et al., 2014). These polymers included natural rubber (Guo et al., 2010; Rooj et al., 2010; Ismail et al., 2013), ethylene propylene diene monomer (EPDM) (Ismail et al., 2008; Pasbakhsh et al., 2010), butadiene–styrene rubber (SBR) (Du et al., 2008; Guo et al., 2008; Jia et al., 2011), polyamide 6 (PA6) (Marney et al., 2008; Guo et al., 2009), polypropylene (PP) (Du et al., 2006, 2010b; Ning et al., 2007; Liu et al., 2008, 2009a,b; Lecouvet et al., 2013c), polyethylene (PE) (Jia et al., 2009; Zhao et al., 2014), epoxy resin (Liu et al., 2007; Ye et al., 2007; Deng et al., 2009; Tang et al., 2011), poly(hydroxybutyrate-co-hydroxyvalerate) (Carli et al., 2014), poly(vinylidene fluoride) (Thakur et al., 2014) *etc.* In general, there are two crucial factors determining the performance of Hal–polymer nanocomposites: a good dispersion of the Hal in the polymer matrix and a desirable interfacial affinity between the Hal and the polymer (Du et al., 2010a; Liu et al., 2014). Although Hal has a good dispersion in aqueous solutions because of the negatively charged external surface and the hydrophilic surface, it remains difficult to achieve a good dispersion of Hal in the polymer matrix and the Hal nanotube readily forms micron-sized aggregates. To enhance the dispersion of Hal in the polymer matrix and the interfacial interactions, Guo et al. (2008) used methacrylic acid (MAA) as a coupling agent to

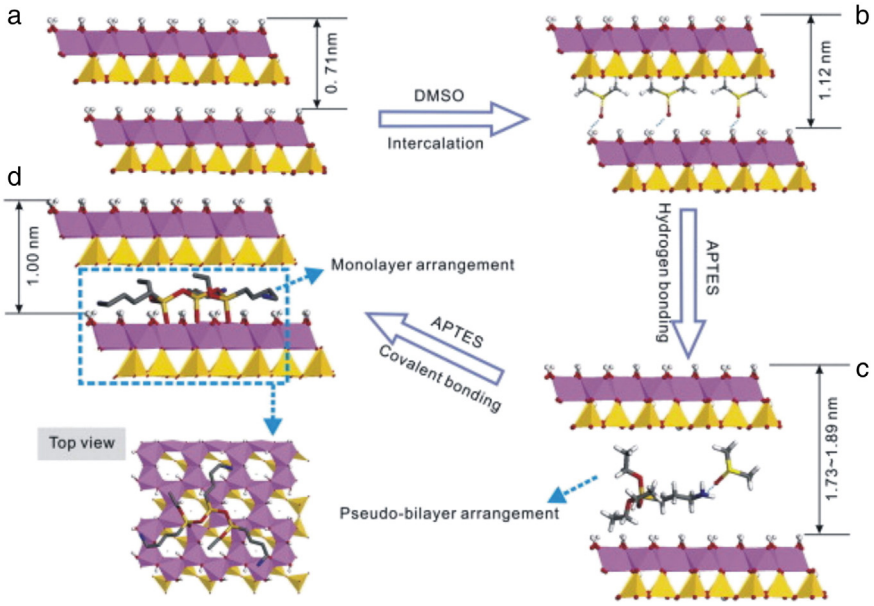

Fig. 9. the interlayer grafting of APTES on kaolinite. Reprinted from Yang et al. (2012) with permission.

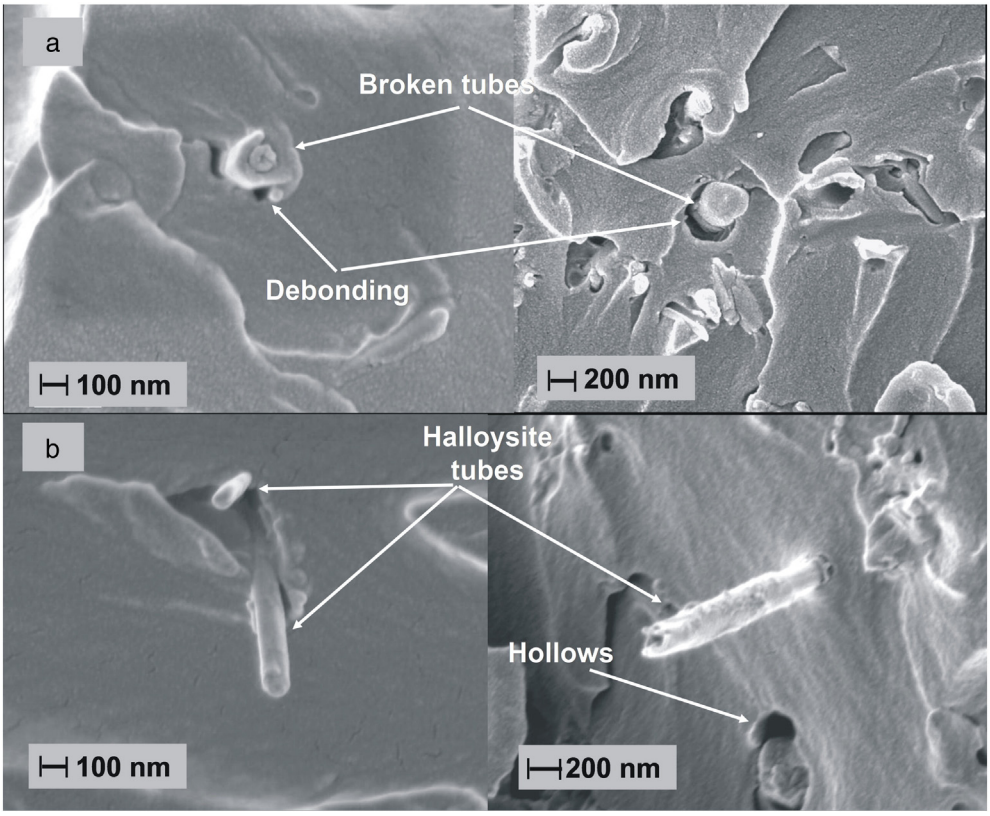

Fig. 10. the TEM image of Hal–polymer nanocomposite. Reprinted from Deng et al. (2009) with permission.

enhance the compatibility between Hal and SBR by direct blending. Hal and SBR generated strong interfacial bonds through zinc methacrylate (ZDMA) and MAA intermediated linkages formed *in situ*. Hal and SBR were connected by ZDMA *via* a grafting/complexation mechanism, and connected by MAA *via* grafting/hydrogen bonding mechanism. Due to the substantial improvement of the dispersion of Hal by virtue of the strong interfacial interactions, the MAA-modified Hal–SBR nanocomposite showed excellent mechanical and vulcanization properties. Pasbakhsh et al. (2010) proposed another way to achieve this purpose by grafting γ-methacryloxypropyl trimethoxysilane on the surface of Hal. This modification increased the interactions between Hal and EPDM and the degree of dispersion of Hal in the EPDM matrix, consequently leading to the improvement of the tensile strength and the tensile modulus.

Overall, the three main effects of Hal addition on the properties of the resulting CPN can be summarized as follows:

i) Hal acted as a reinforcing agent in the CPN and significantly improved its mechanical properties (tensile strength, impact strength, flexural property, *etc.*) (Fig. 10). For instance, Du et al. (2010a) investigated the effect of Hal content on the mechanical property of Hal–PA6 nanocomposites obtained by melt bending. With the increase in Hal content, the flexural strength of the CPN was significantly promoted from 110.0 MPa (neat PA6) to 135.5 MPa (CPN) and the flexural modulus increased from 2711 MPa (neat PA6) to 4557 MPa (CPN); however, the tensile strength and the impact strength were only slightly enhanced. These results were ascribed to the good dispersion of Hal in the PA6 matrix and to the strong interfacial interactions (hydrogen bonding) between the acylamino groups of PA6 and the hydroxyl or the siloxane groups of Hal. Ye et al. (2007) found that bending merely 2.3 mass% Hal into the epoxy matrix could enhance the impact strength by 4 times, from 0.54 kJ/m^2 (neat epoxy) to 2.77 kJ/m^2 (CPN), without a decrease in flexural strength and flexural modulus. This high increase in the impact strength was attributed to the dissipation of the impact energy *via* the nanotube bridging/pulling-out/breaking and *via* the formation of damage zones with a large number of micro-cracks in front of the main crack. This work demonstrated that Hal was an effective impact modifier for some brittle polymers.

ii) Hal acted as a flame-retardant agent, and significantly increased the thermal stability and flame retardancy of the CPN. Du et al. (2006) demonstrated that Hal had drastic effects on the thermal stability of Hal–PP nanocomposites. The decomposition temperature of the CPN was 60 °C higher than that of neat PP. The improvement of flame retardancy by Hal arose from a synergistic effect between physical (*i.e.* ceramic-like structure formation and mechanical reinforcement of the char) and chemical (*i.e.* charring promotion) processes taking place in the condensed phase (Lecouvet et al., 2013b). Some other researchers also ascribed the improvement of flame retardancy to that Hal acted as a barrier against heat and mass transport, as well as from the trapping of polymer decomposition products in the lumen (Lecouvet et al., 2013c; Liu et al., 2014). This improvement in thermal stability and flame retardancy by Hal is also achieved on PA6 (Marney et al., 2008), epoxy (Ye et al., 2007), natural rubber (Rooj et al., 2010), PE (Jia et al., 2009; Zhao et al., 2014), *etc.*

iii) Hal affected the crystallization behavior of semicrystalline polymer, such as PP and PA6 nanocomposites (Ning et al., 2007; Liu et al., 2008, 2009a,b, 2014; Guo et al., 2009; Du et al., 2010b). For instance, the well-dispersed Hal in a PP matrix served as nucleation agents, and accelerated the overall crystallization rate; however, Hal had no effect on the spherulite growth rate because the nucleation and growth of spherulite are two independent processes (Ning et al., 2007). Hal also exerted a great effect

upon the crystallinity of Hal–PA6 nanocomposites. In addition to acting as a nucleating agent and accelerating the crystallization of PA6, Hal could induce the formation of α-phase PA6 during non-isothermal crystallization. The proportion of α-phase PA6 increased with the percentage of Hal in the CPN (Guo et al., 2009).

Apparently, Hal is an effective and low-cost additive and looks promising for use in CPN. However, for the large-scale use of Hal in polymer fabrication, the nonuniform tubule quality of natural Hal must be carefully considered because this inhomogeneity may induce huge quality discrepancies between different batches of CPN. Moreover, the applications of Hal–polymer nanocomposites with high performance in biomedicine, aircraft/automotive manufacture, environmental protection *etc.* should be further developed.

5.2. Support for loading and controlled-release of guests

Hal has great uses as a host for the loading and controlled-release of various guests, including inorganic salts and organic substances ranging from simple organic molecules to high molecular mass biochemical molecules because of its mesoscopic or even macroscopic lumen and high biocompatibility. Price et al. (2001) first used Hal as a carrier for the loading of different types of guest, including tetracycline HCl (hydrophilic), khellin (hydrophobic), and nicotinamide adenine dinucleotide (biochemical). These guests were loaded into the lumen and adsorbed onto the external surface of Hal from the solution or melt. Some inorganic salts, such as silver acetate, ammonium molybdate, potassium permanganate, sodium silicate, and sodium chromate (Abdullayev and Lvov, 2011; Abdullayev et al., 2011), could be loaded into the lumen of Hal from their saturated solution in water *via* vacuum cycling. Moreover, the lumen-loaded silver acetate could be further processed into silver nanorods by thermal decomposition. The Hal/silver composite was proved to be a good filler for paint, which could enhance the tensile strength and endow the paint with antimicrobial activity (Abdullayev et al., 2011).

Based on its molar mass also called molar weight (MW), guests loaded on Hal could be listed in either of the following categories:

i) low MW substances with MW < 300 g/mol, *e.g.*, propranolol hydrochloride (Levis and Deasy, 2003), 5-aminosalicylic (Viseras et al., 2008, 2009; Aguzzi et al., 2013), benzotriazole (Shchukin and Mohwald, 2007; Abdullayev et al., 2009; Abdullayev and Lvov, 2010), 8-hydroxyquinoline (Fix et al., 2009), glycerol (Suh et al., 2011), stearic acid (Mei et al., 2011a), capric acid (Mei et al., 2011b), resveratrol (Vergaro et al., 2012), ibuprofen (Tan et al., 2013, 2014b), and 5-fluorouracil (Rao et al., 2014);
ii) medium MW substances with 300 g/mol < MW < 1000 g/mol, *e.g.*, dexamethasone, furosemide, nifedipine (Veerabadran et al., 2007, 2009), fentanyl (Forsgren et al., 2010), doxorubicin (Mitchell et al., 2012), and orange II (Yuan et al., 2012b);
iii) high MW substances with MW > 1000 g/mol, *e.g.*, metalloporphyrins (Machado et al., 2008), α-amylase (Zhai et al., 2010), urease (Shchukin et al., 2005; Zhai et al., 2010), antisense oligonucleotides (Shi et al., 2011), and insulin (Abdullayev and Lvov, 2011).

Generally, the guest is mainly encapsulated in the lumen, and partly loaded onto the external surface of Hal. The interlayer space of Hal is available for the direct intercalation of some small molecules, *e.g.*, most potassium and ammonium salts, ethylene glycol, glycerin, formamide, DMSO, and phenylphosphonic acid (Carr et al., 1978; Costanzo and Giese, 1986; Hillier and Ryan, 2002; Joussein et al., 2005, 2007; Tang et al., 2011). These substances were classified into three categories by Frost and Kristof (1997): i) compounds that form strong hydrogen bonds with the silicon tetrahedral sheet, such as urea, hydrazine, and acetamide; ii) molecules with strong dipole interactions, which can interact with the silicate layers, such as DMSO; and iii) the alkali salts of short-chain fatty acids, in particular, acetic and propionic acids. In addition to the direct intercalation of the abovementioned substances, the interlayer space of Hal following methoxy-modification is also available for the loading of organic compounds with specific functional groups and/or molecular dimensions (Tan et al., 2015).

The loading capacity of guests on Hal is affected by several factors, such as the morphology of Hal, the pH of the solution, and the solvent. Yuan et al. (2012b) found that Orange II had a higher loading (5.91 mass%) on Hal CLA (see Table 1 for the description of the specimen) than on Hal HG (1.81 mass%). This is because the Hal CLA with a uniform tubular morphology has a higher *SSA* and V_{pore} (49.5 m^2/g and 0.25 cm^3/g) than Hal HG with a low tubular quality (23.2 m^2/g and 0.13 cm^3/g). The pH of the solution also produces a significant effect on the loading of drugs. For instance, the loading content of dexamethasone at pH = 1.4 was 5.5 mass%, much higher than at pH = 9.4 (2.0 mass%). This occurred because at lower pH the drug had a higher solubility and the lumen of Hal had an increased positive charge (Abdullayev and Lvov, 2011).

The release of guests from Hal depends on the physico-chemical property of the guest and on the interactions between the guest and the host. The complete release of inorganic salts from Hal is accomplished within 1–2 h, much faster than the release of organic compounds (Abdullayev and Lvov, 2011). This is because inorganic salts have a higher solubility in water, a greater mobility, and weaker interactions with Hal. The release of organic compounds from Hal has a close relationship with the MW and the number of functional groups in the organic compounds. For instance, guests with low MW, *e.g.*, propranolol hydrochloride (Levis and Deasy, 2003), could be completely released in 2–10 h because the large lumen of Hal had little limitation for the diffusion of such a guest with small molecular dimensions. Veerabadran et al. (2007) investigated the loading and release of medium MW substances (dexamethasone, furosemide, and nifedipine) on Hal. The complete release of furosemide, dexamethasone, and nifedipine bulk crystals occurred in 15, 30, and 40 min, respectively. However, due to the confinement of the lumen and the interactions between Hal and the drugs, the release of these drugs was 20 times slower than in bulk. In addition, the release of nifedipine was the slowest because nifedipine has the highest number of functional groups among the three drugs and therefore the strongest interactions with Hal. However, the release of high MW substances, *e.g.*, proteins and polymers, could last 100–500 h. For instance, only 70% of insulin was released within 140 h. This slow release was ascribed to the large diameter (2 nm) and the high number of functional groups of insulin, which generated a slow diffusion in water and strong interactions with Hal (Abdullayev and Lvov, 2011).

Generally, due to the weak interactions (ion exchange, hydrogen bonding, and van der Waals forces) and the fast outward diffusion of the lumen-loaded guest, the guest exhibited a fast release behavior on Hal. This drawback seriously restricted the application of Hal as carrier in long-term release fields. Theoretically, prolonging the release of the guest from Hal can be achieved by enhancing the interactions between the Hal and the guest and by slowing the outward diffusion of the guest. For example, ibuprofen only participated in hydrogen bonding and van der Waals interactions with unmodified Hal, resulting in a fast release; however, in the case of APTES-modified Hal, ibuprofen and the modified Hal interacted *via* electrostatic attraction between the carboxylate ($-COO^-$) of ibuprofen and the protonated aminopropyl group ($-NH_3^+$) of the grafted APTES, which was formed by proton transfer from the carboxyl groups of ibuprofen to the aminopropyl groups of the grafted APTES. This strong interaction prolonged the release of ibuprofen (Fig. 11), which was achieved by introducing more encapsulated ibuprofen into the lumen and by retarding the dissolution and diffusion

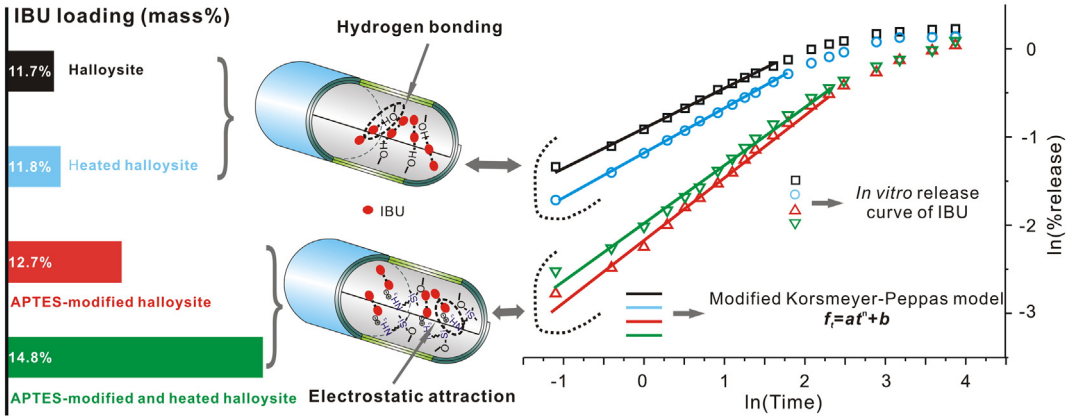

Fig. 11. Schematic representation of the effect of APTES modification on the loading and release of ibuprofen on Hal. Reprinted from Tan et al. (2014b) with permission.

of ibuprofen from the lumen of the APTES-modified Hal (Tan et al., 2014b).

Two approaches have been proposed to slow the outward diffusion of guests from Hal: i) LBL assembly of polyelectrolytes shells on Hal and ii) formation of stoppers at the tube end.

Veerabadran et al. (2009) alternately assembled polycations (PAH, PEI, and chitosan) and polyanions (PSS, PAA, and gelatin) on the external surface of pre-loaded Hal to form organized shells. The organized shell acted as a diffusion barrier and significantly decreased the release of dexamethasone from Hal. In addition, this retardation of the diffusion of dexamethasone was significantly related to i) the type of polyelectrolytes, strong polyelectrolytes with a high degree of ionization (PEI and PSS) offered a remarkable retardation of diffusion as compared with weak polyelectrolytes (PAH and PAA) and ii) the MW of the coated polyelectrolytes, with the release of dexamethasone decreased with the increasing MW of polyelectrolyte.

Creating stoppers at the tube end is another approach to retard the outward diffusion of guests from the lumen and was first proposed by Lvov's group. The stopper could be a precipitate or insoluble complex, formed by the reaction between the loaded agent and the sealed agent. The presence of stoppers could significantly slow the release of the loaded agent by reducing the outward diffusion process (Fig. 12). This approach was first proposed by Abdullayev and Lvov (2010) when they loaded the corrosion inhibitor benzotriazole into the lumen of Hal and then rinsed it with a transition metal (Fe^{2+}, Co^{2+}, Cu^{2+}) salt solution. The benzotriazole reacted with the metal ions to form thin films that capped the tube ends and acted as stoppers. The benzotriazole hardly released from the lumen under the suppression effect of the stoppers. However, the release of benzotriazole could be triggered by the addition of concentrated ammonia solution because the metal ions form more stable but soluble complexes with ammonia; the stoppers were then opened and the benzotriazole was released from the lumen of Hal.

5.3. Adsorbent for pollution remediation

Naturally occurring porous minerals as adsorbents for the remediation of environmental pollution have been listed as one of the hottest topics in environmental science as well as material science because of the economic viability and the desirable properties of porous minerals such as high SSA and excellent adsorption capacity. Microporous (with pore size smaller than 2 nm) minerals such as zeolite (Motsi et al., 2009) and montmorillonite (Yuan et al., 2009) as well as macroporous minerals (pore size > 50 nm) such as diatomite have been widely used for the removal of various contaminants from aqueous solutions (Yuan et al., 2010). Curiously, the use of tubular Hal for applications in environmental remediation has not received much attention until the last decade during which a resurgence of interest in this topic occurred. A possible reason for this previous lack of interest is the chemical similarity of tubular Hal to platy Kaol, which was thought a less reactive adsorbent for contaminants such as heavy metal cations in comparison with other clay minerals with a high cationic exchange capacity (CEC) such as montmorillonite. With a better understanding of the structure and reactivity of Hal, it has been gradually realized that Hal possesses several properties that are advantageous for contaminant adsorption. For example, the SSA of nanosized

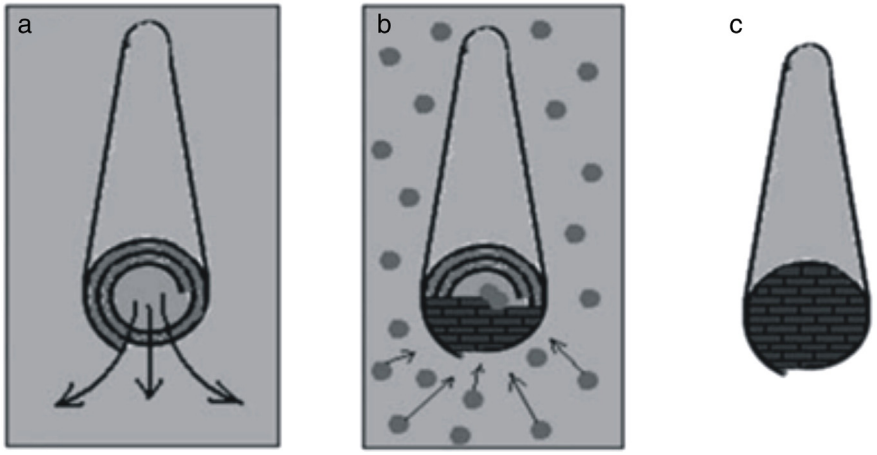

Fig. 12. Schematic representation of the formation tube stoppers on the Hal. Reprinted from Abdullayev and Lvov (2010) with permission.

porous Hal is normally much higher than that of micron-sized non-porous Kaol; moreover, Hal has multiple surface groups, external siloxane groups, interlayer inner-surface aluminol groups, and internal aluminol groups, which allow for diverse post-modification possibilities to improve the performance of Hal as adsorbent for contaminants.

Exposure to excessive amounts of harmful metals constitutes a great threat to human health and may sometimes lead to serious health problems even at trace concentrations, although some heavy metals such as zinc and copper are important nutrients needed in small quantities. Therefore, removing hazardous heavy metals from aqueous media is of high environmental importance, and the adsorption-based route is among the most used techniques for the remediation of heavy metal pollution. Kilislioglu and Bilgin (2002) studied the adsorption of uranium, U(VI), from aqueous solutions on Hal as a function of initial U(VI) concentrations, amounts of adsorbent, and pH. The results show that the adsorption of U(VI) by Hal was endothermic and occurred more spontaneously at high temperature. Instead of directly using Hal powder in the adsorption study, Wang et al. (2014a) prepared a molded material of Hal-alginate hybrid beads, which they applied to a continuous fixed bed adsorption of Cu(II). The results showed that the adsorption capacity of the hybrid beads reached 74.1 mg/g when the initial inlet concentration of Cu(II) was 100 mg/L with a bed height of 12 cm and flow rate of 3 mL/min. The hybrid material exhibited a good performance for regeneration because it retained a high adsorption capacity after 3 adsorption–desorption cycles.

In principle, the adsorption of metal ions on raw Hal usually takes place *via* ion exchange and surface complexation at permanently charged and pH-dependent variable charge sites. However, the adsorption was relatively low because the interlayer space of Hal is originally not accessible to ions and molecules unlike montmorillonite, whose interlayer space readily accommodates cations. Matusik and Wścisło (2014) showed that the efficiency of heavy metal uptake by Hal was influenced by the hydrolysis constant of the metals and that the removal followed the sequence Pb(II) > Cu(II) > Zn(II) ≈ Cd(II), although the overall adsorption capacities of these ions in Hal was low. For this purpose, these authors proposed to use interlayer grafted Hal as adsorbent for the mentioned metal ions. Diethanolamine (DEA, $(CH_2CH_2OH)_2NH$) and triethanolamine (TEA, $(CH_2CH_2OH)_3N$) were intercalated into the interlayer space of Hal, resulting in stable interlayer distances of 3.1 Å and 3.6 Å, respectively (Fig. 13a, b). The intercalation modification substantially improved the Hal adsorption capacity (*e.g.*, the adsorption capacity increased by approximately 10 times for Cd(II)) with respect to the above-mentioned metal ions, mainly due to the amine nitrogen of DEA or TEA grafted in the interlayer of Hal acting as an additional site for ion adsorption. Specifically, the improvement in metal removal was attributed to a two-steps gradual diffusion of the ions into the interlayer space and the subsequent attraction by the amine nitrogen. It is of particular interest that the Cu(II) ions were found to be preferentially removed from the solution as they readily form complexes with N-donor ligands (Fig. 13c, d).

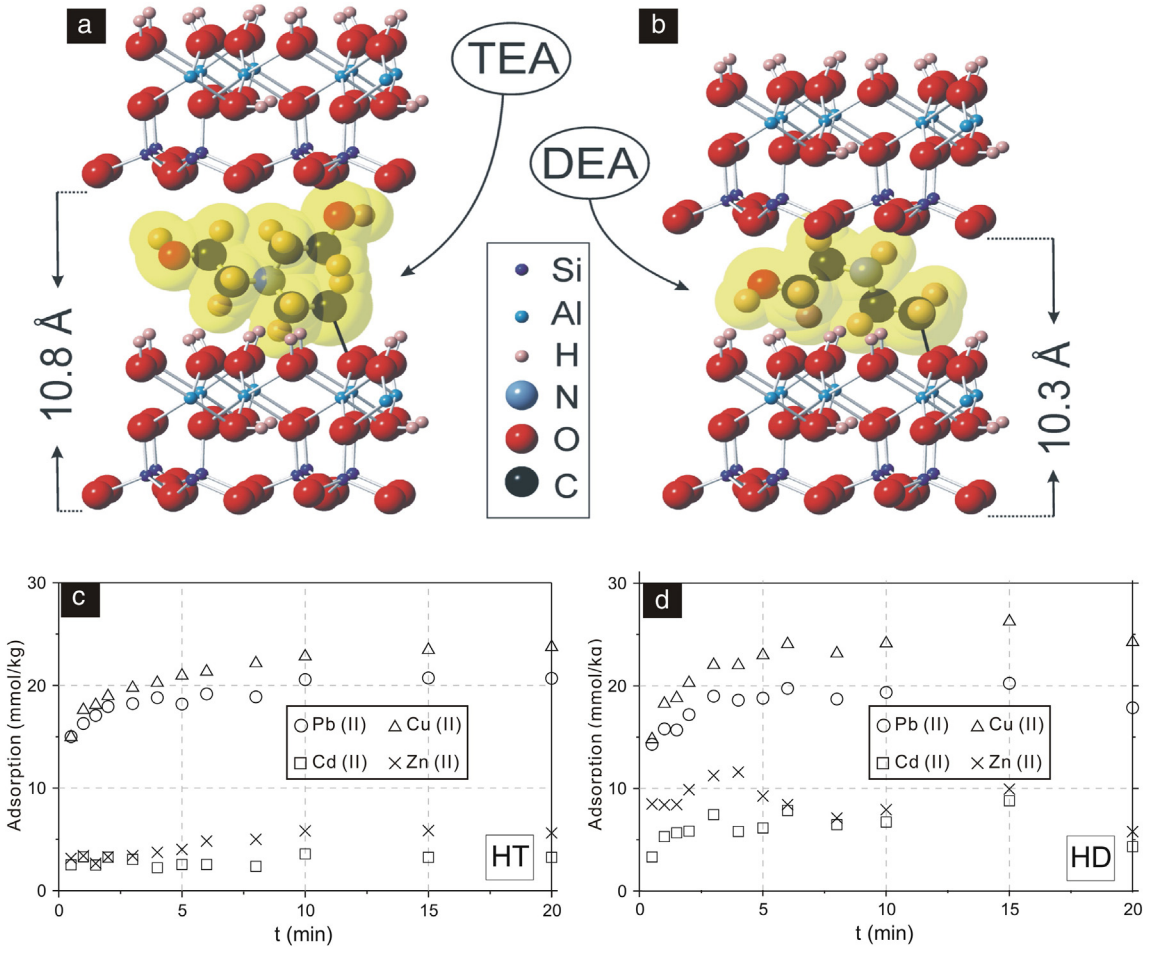

Fig. 13. The structure model of the (a) TEA-modified Hal and (b) DEA-modified Hal, and the kinetics of Pb(II), Cd(II), Zn(II), and Cu(II) uptake in (c) TEA-modified Hal and (d) DEA-modified Hal samples. Adapted from Matusik and Wścisło (2014) with permission.

The effects of the intercalation of acetates $M^{n+}(CH_3COO)_n$ ($M = Na^+$, NH_4^+ or Pb^{2+}) on Cu(II) adsorption by Hal was also studied by Mellouk et al. (2009). These authors found that Cu(II) adsorption by the $NaCH_3COO$ intercalated Hal was approximately 2.2 times larger than that by the non-intercalated Hal. This increase in adsorption capacity was explained by cation exchange on negative surface sites and cation exchange associated with the intercalated acetate. In addition to interlayer modification, external surface modifications using hexadecyltrimethylammonium bromide (HDTMA) was also applied for metal ions adsorption. Wang et al. (2010) reported the removal of Cr(VI) from its aqueous solution by HDTMA-modified Hal, which exhibited a rapid adsorption rate for chromates, approaching 90% of its maximum adsorption capacity within 5 min. The adsorption process was primarily driven by the electrostatic attraction between the surfactant cations and the Cr(VI) anions $HCrO_4^-$ and $Cr_2O_7^{2-}$. Duan et al. (2010) also proposed a method for the removal of Cr(VI) by Hal materials modified with γ-mercaptopropyltrimethoxy silane, however, the Cr(VI) adsorption capacity was somewhat low, 2.79 mg/g, and the mechanism of the reaction of silane with Cr(VI) anions was not given. Moreover, Ballav et al. (2014) investigated the performance of polypyrrole-coated Hal as adsorbent for Cr(VI), and found that the Cr(VI) adsorption on polypyrrole-coated Hal was spontaneous and endothermic in nature; the maximum adsorption capacity was as high as 149.25 mg/g at pH 2.0, and some part of Cr(VI) was reduced to Cr(III) by electron-rich polypyrrole moiety.

Organic contaminants are also widely produced from industrial processes, and many of them are very harmful to human beings and microorganisms. The removal of organic contaminants from aqueous solutions has therefore received considerable attention in recent decades. Synthetic dyes are the most studied organic contaminants using Hal as adsorbent, most likely because they are widely used in various industries such as paper, textile, leather, printing, food, and plastic, and their discharge into water causes serious environmental problem, related to their carcinogenicity or toxicity to aquatic life and human beings (Liu et al., 2012). The adsorption of a series of dye molecules, including methylene blue (Zhao and Liu, 2008; Luo et al., 2011; Zhang et al., 2012b), neutral red (Luo et al., 2010), methyl violet (Liu et al., 2011), methyl orange (Xie et al., 2011; Li et al., 2015), and malachite green (Kiani et al., 2011) by Hal has been reported. Generally, the results demonstrated that Hal could be used as an effective low-cost adsorbent for the removal of dye contaminants from wastewater, although the adsorption capacity is relatively low in comparison to other synthetic high surface area adsorbent such as activated porous carbon (Liu et al., 2013) and mesoporous silica. The adsorption of dye molecules on Hal depends on the adsorption conditions, including adsorbent dose, temperature, initial pH, ionic strength, and contact time. Regarding the solid–liquid separation after the adsorption, Xie et al. (2011) proposed a convenient magnetic separation rather than the commonly used filtration or centrifugation processes. In this study, magnetic Fe_3O_4 nanoparticles were deposited on the surface of Hal to enable the product magnetic to react to an extra magnetic field. This method is comparable with the previously reported method for the preparation of hybrid Fe_3O_4/montmorillonite or Fe_3O_4/diatomite materials.

In addition to synthetic dyes, the adsorption of organic contaminants such as naphthalene (Lee and Kim, 2002), ammonium (Zheng and Wang, 2010), and chloroaniline (Szczepanik et al., 2014) by Hal has also been studied. HDTMA modification was used to improve naphthalene adsorption by Hal because naphthalene is hydrophobic. For the adsorption of ammonium, a hybrid CPN composed of Hal, chitosan, and acrylic acid exhibited well-formed three-dimensional polymeric networks with a high adsorption capacity, rapid adsorption kinetics, and good regenerability for ammonium removal. In the case of chloroanilines, acid-activated Hal was used as the adsorbent for the removal of 3-,4-chloroaniline and 3,4-dichloroaniline from aqueous solution. The chloroanilines were chemically adsorbed on Hal and fitted with a pseudo-second order kinetic model.

The tendency to abuse antibiotics in some developing countries and the subsequent improper disposal has resulted in potential threat to aquatic organisms and human health *via* the food chain, causing a growing concern on this issue. Wang et al. (2014b) investigated the adsorption of ofloxacin on Hal, and found that the adsorption occurred *via* electrostatic interactions between protonated ofloxacin and the negative Hal surface. Dai et al. (2014) prepared a highly controllable core–shell hybrid nanomaterial based on magnetically modified Hal for tetracycline adsorption. A desirable selective recognition and rapid adsorption of tetracycline from aqueous solution was achieved by using this nanomaterial, which also exhibits good stability and regeneration property, enabling its potential use in practical applications not only for wastewater treatment but also for other uses such as the purification of biological molecules and drug extraction. In a study conducted by Zhang et al. (2014), the application of modified Hal in reducing the toxic effect of zearalenone in rats by adsorption was demonstrated, and the result suggested that Hal can be used as additive in animal feed for zearalenone adsorption. In addition to the above-mentioned uses for liquid contaminants in environmental remediation, Hal was also used for the adsorption of ionic liquids such as 1-butyl-3-methyl-imiazolium hexafluorophosphate (Guo et al., 2010); the interaction between this type of ionic liquid and Hal was proposed to be hydrogen bonding. When used for the preparation of a Hal-rubber nanocomposite, the products with ionic liquid modified Hal showed significantly faster curing and the resulting vulcanizates showed substantially higher tensile strength and much lower hardness. The adsorptive properties of Hal have also been shown to have uses in analysis techniques such as inverse gas chromatography. Czech and Slomkiewicz (2013) reported the fast measurement of dichloroethylene, trichloroethylene, and tetrachloroethylene using acid-activated Hal as adsorbent. More applications making use of the adsorptive properties of Hal are reported in the following section.

5.4. Nanoreactor/nanotemplate for synthesis of hybrid functional materials

In addition to being a space for the loading of guests, the mesoporous lumen of Hal can also act as a nanoreactor/nanotemplate for biomimetic synthesis at the nanoscale. Shchukin et al. (2005) first used Hal nanotubes as an enzymatic nanoreactor for the biomimetic synthesis of $CaCO_3$ (Fig. 14). Urease was first embedded into the lumen of Hal, and the product was dipped into a solution containing a high concentration of $CaCl_2$ and urea. The urea decomposed into ammonia and CO_3^{2-} by the *in situ* catalysis of the lumen-loaded urease. Then, precipitation of $CaCO_3$ occurred in the lumen of Hal. Due to the exclusive loading of urease into the lumen, the $CaCO_3$ precipitate completely filled the lumen as a metastable vaterite phase, resulting from the influence of the confined reaction nanovolume on the polymorph modification of $CaCO_3$. This idea enlightens promising possibilities for studying crystal engineering and fundamental aspects of the biomineralization process. Based on the nanotubular structure, Hal has also been used as a nanotemplate to synthesize porous carbon. The porous carbon was obtained *via* the polymerization and carbonization of a carbon precursor (sucrose, furfuryl alcohol, *etc.*) with Hal and subsequent demineralization using HF and HCl to remove the Hal template (Liu et al., 2006; Wang et al., 2006, 2008; Huang et al., 2010). The mesoporous carbon replicated the tubular morphology of the Hal template and exhibited tubular, rod, as well as the dominant nanosheet morphology, which was caused by the carbon precursor being mostly deposited on the external surface of the Hal. The resulting mesoporous carbon exhibited a high degree of mesoporosity (78–84%), high *SSA* (1130 m^2/g), and large V_{pore} (2.32 cm^3/g). This porous carbon also had a high specific capacitance (232 F/g) and could be used as a promising double layer electric capacitor. In addition, Hal was also used as template to fabricate some metallic or polymeric nanoparticles/nanowires (Baral et al., 1993; Fu and Zhang, 2005a; Fu et al., 2005b; Zhang and Liu, 2008; Li et al., 2009). For instance, Fu and Zhang (2005a) demonstrated that amorphous Ni nanoparticles (within a diameter of 20–30 nm) were deposited onto

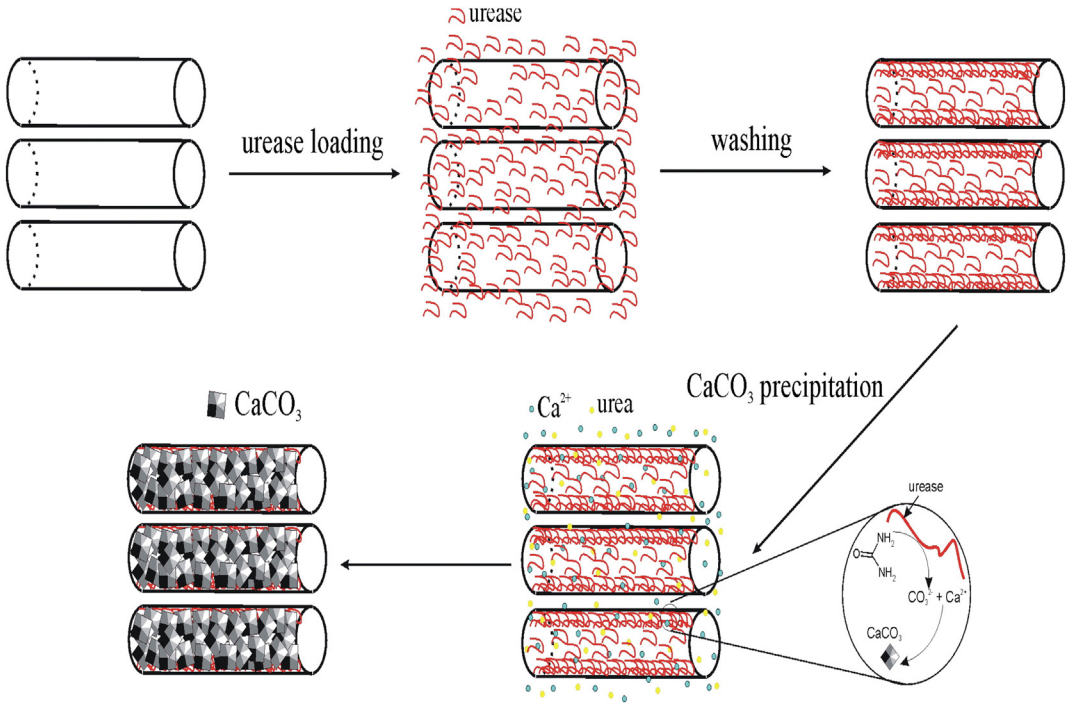

Fig. 14. Schematic illustration of the urease-catalyzed synthesis of $CaCO_3$ inside Hal nanotubes. Reprinted from Shchukin et al. (2005) with permission.

the external surface of Hal and that some discontinuous Ni nanowires (approximately 15 nm in diameter) were simultaneously deposited into the lumen of Hal. The Ni wire was in a super-paramagnetic state because the size of the Ni wire was far smaller than the size of a single magnetic domain of Ni (20–40 nm). Consequently, there was no contribution of the Ni wire to the magnetic property of the Ni/Hal nanocomposite.

6. Conclusion

Overall, three main properties and related applications of Hal are summarized from the literature:

(1) The first property is the nanosized hollow tubular structure with one-dimensional mesoporosity or macroporosity, enabling the encapsulation of various active guests in the lumen of Hal that acts as a nanoscale container, as well as the subsequent controlled release of the guests. The Hal nanotube is also an effective nanofiller in CPN because Hal is naturally dispersed, unlike the traditional micron-sized counterparts such as glass fibers and other clay mineral nanofillers such as montmorillonite that have to undergo exfoliation pretreatments to produce nanolayers. Moreover, the hollow structure is quite useful for decreasing the density of CPN and for a lower loading that still achieves equivalent properties. A drawback of these applications is that the morphological properties (length, external diameter, internal diameter, and wall thickness) of Hal significantly affect its performance in these applications, and the morphology and structure of natural Hal are highly variable and dependent on the deposits. This means that the purification and size classification techniques from the perspective of mineral processing need to be developed in the future. In addition, there are already some research advances on the preparation of Hal-like nanotubes with high purity and morphological uniformity *via* the delamination of Kaol; however, the production remains on the laboratory scale, and new preparation routes with better productivity and cost-saving properties deserve to be studied.

(2) The second property is the controllable surface reactivity with site-dependent availability for post-modification. In principle, the surface groups of Hal can be divided into two types. One type is the easily available surface group including the internal lumen (cylindrical channel) aluminol groups and the external siloxane surface of the tubules. The second type is the aluminol group at the interlayer surface. The former affects the surface charge of Hal through the combined action of pH-dependent variable charge and constant negative charges, resulting in a significant influence on the aggregation and dispersion of Hal nanotubes in aqueous dispersions as well as the interactions between Hal and charged guests especially in adsorption or environmental remediation applications. Compared with the understanding of the internal and external surfaces, the interlayer host–guest chemistry of Hal is not yet clearly understood. However, there is no doubt that much more attention deserves to be paid to this topic because the availability of the interlayer space of Hal for hosting guests may enable many new applications such as loading, controlled release, adsorption, and catalysis; moreover, the applications of Hal can even be further extended, especially for uses as hybrid materials with novel functionalities. In particular, techniques to introduce different functionalities such as variable hydrophobicity or hydrophilicity, controllability, or selectivity *via* separate modifications to the different surfaces of Hal would be highly meaningful and are still subjects to be developed.

(3) The last property is the structural stability and phase transformation of Hal under thermal or acid/base treatments. The high-temperature-resistant property of Hal is useful for applications in producing advanced ceramics with special properties. The finding that calcination at 600–900 °C creates new hydroxyl groups on the external surface, which is now available for grafting modifications might find uses in hybrid materials or guest adsorption or loading. The significant increase in the SSA and V_{pore} of Hal after strong acid or base treatments help to improve the adsorption performance of treated Hal products in related adsorption applications and

most likely for encapsulation-related uses because of the enlargement of the lumen space. A combination of different processing techniques has to be carefully selected to cater for the specific requirements of a target industry.

In conclusion, this review highlights that tubular Hal is a low-cost, natural material having many interesting properties that allow for versatile potential uses in a variety of domains. Future studies should pay more attention to the unresolved fundamental structure and properties, as well as to the reasonable combination of methods based on the already obtained knowledge to develop novel Hal-related hybrid materials for high efficiency applications of the precious Hal resource.

Acknowledgment

Financial supports from the Team Project of Natural Science Foundation of Guangdong Province, China (S2013030014241) and the National Natural Science Foundation of China (Grant Nos. 41472045 and 41072032) are gratefully acknowledged. This is a contribution (No. IS-2061) from GIGCAS.

References

Abdullayev, E., Lvov, Y., 2010. Clay nanotubes for corrosion inhibitor encapsulation: release control with end stoppers. J. Mater. Chem. 20 (32), 6681–6687.
Abdullayev, E., Lvov, Y., 2011. Halloysite clay nanotubes for controlled release of protective agents. J. Nanosci. Nanotechnol. 11 (11), 10007–10026.
Abdullayev, E., Price, R., Shchukin, D., Lvov, Y., 2009. Halloysite tubes as nanocontainers for anticorrosion coating with benzotriazole. ACS Appl. Mater. Interfaces 1 (7), 1437–1443.
Abdullayev, E., Sakakibara, K., Okamoto, K., Wei, W.B., Ariga, K., Lvov, Y., 2011. Natural tubule clay template synthesis of silver nanorods for antibacterial composite coating. ACS Appl. Mater. Interfaces 3 (10), 4040–4046.
Abdullayev, E., Joshi, A., Wei, W.B., Zhao, Y.F., Lvov, Y., 2012. Enlargement of halloysite clay nanotube lumen by selective etching of aluminum oxide. ACS Nano 6 (8), 7216–7226.
Adamo, P., Violante, P., Wilson, M.J., 2001. Tubular and spheroidal halloysite in pyroclastic deposits in the area of the Roccamonfina volcano (Southern Italy). Geoderma 99 (3-4), 295–316.
Aguzzi, C., Viseras, C., Cerezo, P., Salcedo, I., Sánchez-Espejo, R., Valenzuela, C., 2013. Release kinetics of 5-aminosalicylic acid from halloysite. Colloids Surf. B 105, 75–80.
Antill, S.J., 2003. Halloysite: a low-cost alternative nanotube. Aust. J. Chem. 56 (7), 723-723.
Bailey, S.W., 1990. Halloysite — a critical assessment. Sci. Geol. Mem. 86, 89–98.
Ballav, N., Choi, H.J., Mishra, S.B., Maity, A., 2014. Polypyrrole-coated halloysite nanotube clay nanocomposite: synthesis, characterization and Cr(VI) adsorption behaviour. Appl. Clay Sci. 102, 60–70.
Baral, S., Brandow, S., Gaber, B.P., 1993. Electroless metalization of halloysite, a hollow cylindrical 1:1 aluminosilicate of submicron diameter. Chem. Mater. 5 (9), 1227–1232.
Bates, T.F., Hildebrand, F.A., Swineford, A., 1950. Morphology and structure of endellite and halloysite. Am. Mineral. 35 (7-8), 463–484.
Bergaya, F., Dion, P., Alcover, J.F., Clinard, C., Tchoubar, D., 1996. TEM study of kaolinite thermal decomposition by controlled-rate thermal analysis. J. Mater. Sci. 31 (19), 5069–5075.
Berthier, P., 1826. Analyse de l'halloysite. Ann. Chim. Phys. 32, 332–335.
Brindley, G.W., Nakahira, M., 1959. The kaoiinite–mullite reaction series: I, A survey of outstanding problems. J. Am. Ceram. Soc. 42 (7), 311–314.
Brindley, G.W., Robinson, K., 1946. Randomness in the structures of kaolinitic clay minerals. Trans. Faraday Soc. 42, B198–B205.
Brindley, G.W., Robinson, K., Goodyear, J., 1949. X-Ray studies of halloysite and metahalloysite. 3. The effect of temperature and pressure on the halloysite–metahalloysite transition. Am. Mineral. 34 (3-4), 423–428.
Brown, I.W.M., MacKenzie, K.J.D., Bowden, M.E., Meinhold, R.H., 1985. Outstanding problems in the kaolinite–mullite reaction sequence investigated by ^{29}Si and ^{27}Al solid-state Nuclear Magnetic Resonance: 11, high-temperature transformations of metakaolinite. J. Am. Ceram. Soc. 68 (6), 298–301.
Carli, L.N., Daitx, T.S., Soares, G.V., Crespo, J.S., Mauler, R.S., 2014. The effects of silane coupling agents on the properties of PHBV/halloysite nanocomposites. Appl. Clay Sci. 87, 311–319.
Carr, R.M., Chaikum, N., Patterson, N., 1978. Intercalation of salts in halloysite. Clay Clay Miner. 26 (2), 144–152.
Chang, P.R., Xie, Y.F., Wu, D.L., Ma, X.F., 2011. Amy lose wrapped halloysite nanotubes. Carbohydr. Polym. 84 (4), 1426–1429.
Churchman, G.J., Davy, T.J., Aylmore, L.A.G., Gilkes, R.J., Self, P.G., 1995. Characteristics of fine pores in some halloysites. Clay Miner. 30 (2), 89–98.
Costanzo, P.M., Giese, R.F., 1986. Ordered halloysite — dimethylsulfoxide intercalate. Clay Clay Miner. 34 (1), 105–107.
Czech, K., Slomkiewicz, P.M., 2013. Determination of adsorption isotherms of chlorinated hydrocarbons on halloysite adsorbent by inverse gas chromatography. J. Chromatogr. A 1288, 96–100.
Dai, J., Wei, X., Cao, Z., Zhou, Z., Yu, P., Pan, J., Zou, T., Li, C., Yan, Y., 2014. Highly-controllable imprinted polymer nanoshell at the surface of magnetic halloysite nanotubes for selective recognition and rapid adsorption of tetracycline. RSC Adv. 4 (16), 7967–7978.
de Faria, E.H., Lima, O.J., Ciuffi, K.J., Nassar, E.J., Vicente, M.A., Trujillano, R., Calefi, P.S., 2009. Hybrid materials prepared by interlayer functionalization of kaolinite with pyridine-carboxylic acids. J. Colloid Interface Sci. 335 (2), 210–215.
de Faria, E.H., Ciuffi, K.J., Nassar, E.J., Vicente, M.A., Trujillano, R., Calefi, P.S., 2010. Novel reactive amino-compound: tris(hydroxymethyl)aminomethane covalently grafted on kaolinite. Appl. Clay Sci. 48 (3), 516–521.
de Faria, E.H., Nassar, E.J., Ciuffi, K.J., Vicente, M.A., Trujillano, R., Rives, V., Calefi, P.S., 2011. New highly luminescent hybrid materials: terbium pyridine–picolinate covalently grafted on kaolinite. ACS Appl. Mater. Interfaces 3 (4), 1311–1318.
Deng, S., Zhang, J., Ye, L., 2009. Halloysite–epoxy nanocomposites with improved particle dispersion through ball mill homogenisation and chemical treatments. Compos. Sci. Technol. 69 (14), 2497–2505.
Dion, P., Alcover, J.F., Bergaya, F., Ortega, A., Llewellyn, P.L., Rouquerol, F., 1998. Kinetic study by controlled-transformation rate thermal analysis of the dehydroxylation of kaolinite. Clay Miner. 33 (2), 269–276.
Djemai, A., Balan, E., Morin, G., Hernandez, G., Labbe, J.C., Muller, J.P., 2001. Behavior of paramagnetic iron during the thermal transformations of kaolinite. J. Am. Ceram. Soc. 84 (5), 1017–1024.
Du, M.L., Guo, B.C., Jia, D.M., 2006. Thermal stability and flame retardant effects of halloysite nanotubes on poly(propylene). Eur. Polym. J. 42 (6), 1362–1369.
Du, M.L., Guo, B., Lei, Y., Liu, M., Jia, D., 2008. Carboxylated butadiene–styrene rubber/halloysite nanotube nanocomposites: interfacial interaction and performance. Polymer 49 (22), 4871–4876.
Du, M.L., Guo, B.C., Jia, D.M., 2010a. Newly emerging applications of halloysite nanotubes: a review. Polym. Int. 59 (5), 574–582.
Du, M.L., Guo, B.C., Wan, J.J., Zou, Q.L., Jia, D.M., 2010b. Effects of halloysite nanotubes on kinetics and activation energy of non-isothermal crystallization of polypropylene. J. Polym. Res. 17 (1), 109–118.
Duan, J., Wang, J., Zhang, B., Zhao, Y., Liu, J., 2010. Cr(VI) adsorption on mercaptopropyl-functionalized halloysite nanotubes. Fresenius Environ. Bull. 19 (12), 2783–2787.
Ece, Ö.I., Schroeder, P.A., 2007. Clay mineralogy and chemistry of halloysite and alunite deposits in the Turplu area, Balikesir, Turkey. Clay Clay Miner. 55 (1), 18–35.
Fix, D., Andreeva, D.V., Lvov, Y.M., Shchukin, D.G., Moehwald, H., 2009. Application of inhibitor-loaded halloysite nanotubes in active anti-corrosive coatings. Adv. Funct. Mater. 19 (11), 1720–1727.
Forsgren, J., Jamstorp, E., Bredenberg, S., Engqvist, H., Stromme, M., 2010. A ceramic drug delivery vehicle for oral administration of highly potent opioids. J. Pharm. Sci. U.S. 99 (1), 219–226.
Frost, R.L., Kristof, J., 1997. Intercalation of halloysite: a Raman spectroscopic study. Clay Clay Miner. 45 (4), 551–563.
Frost, R.L., Vassallo, A.M., 1996. The dehydroxylation of the kaolinite clay minerals using infrared emission spectroscopy. Clay Clay Miner. 44 (5), 635–651.
Fu, Y.B., Zhang, L.D., 2005. Simultaneous deposition of Ni nanoparticles and wires on a tubular halloysite template: a novel metallized ceramic microstructure. J. Solid State Chem. 178 (11), 3595–3600.
Fu, Y.B., Zhang, L.D., Zheng, J.Y., 2005. In-situ deposition of Pd nanoparticles on tubular halloysite template for initiation of metallization. J. Nanosci. Nanotechnol. 5 (4), 558–564.
Gardolinski, J.E.F.C., Lagaly, G., 2005. Grafted organic derivatives of kaolinite: II. Intercalation of primary n-alkylamines and delamination. Clay Miner. 40 (4), 547–556.
Giese, R., 1988. Kaolin minerals; structures and stabilities. Rev. Mineral. Geochem. 19 (1), 29–66.
Guimaraes, L., Enyashin, A.N., Seifert, G., Duarte, H.A., 2010. Structural, electronic, and mechanical properties of single-walled halloysite nanotube models. J. Phys. Chem. C 114 (26), 11358–11363.
Guo, B., Lei, Y., Chen, F., Liu, X., Du, M., Jia, D., 2008. Styrene–butadiene rubber/halloysite nanotubes nanocomposites modified by methacrylic acid. Appl. Surf. Sci. 255 (5, Part 2), 2715–2722.
Guo, B., Zou, Q., Lei, Y., Du, M., Liu, M., Jia, D., 2009. Crystallization behavior of polyamide 6/halloysite nanotubes nanocomposites. Thermochim. Acta 484 (1–2), 48–56.
Guo, B., Liu, X., Zhou, W.Y., Lei, Y., Jia, D., 2010. Adsorption of ionic liquid onto halloysite nanotubes: mechanism and reinforcement of the modified clay to rubber. J. Macromol. Sci. B 49 (5), 1029–1043.
Hendricks, S.B., Jefferson, M.E., 1938. Structures of kaolin and talc-pyrophyllite hydrates and their bearing on water sorption of the clays. Am. Mineral. 23 (12), 863–875.
Hillier, S., Ryan, P.C., 2002. Identification of halloysite (7 angstrom) by ethylene glycol solvation: the 'MacEwan effect'. Clay Miner. 37 (3), 487–496.
Honjo, G., Kitamura, N., Mihama, K., 1954. A study of clay minerals by means of single crystal electron diffraction diagrams—the structure of tubular kaolin. Clay Miner. Bull. 2, 133–141.
Huang, Z.H., Wang, A., Kang, F., Chuan, X., 2010. Mesoporous carbon nanosheets derived from tubular halloysite and furfuryl alcohol with different concentrations. Mater. Lett. 64 (22), 2444–2446.
Hughes, I., Pottery, N.Z., Association, C.R., 1966. Mineral changes of halloysite on drying. New Zealand Pottery and Ceramics Research Association.

Ismail, H., Pasbakhsh, P., Fauzi, M.N.A., Abu Bakar, A., 2008. Morphological, thermal and tensile properties of halloysite nanotubes filled ethylene propylene diene monomer (EPDM) nanocomposites. Polym. Test. 27 (7), 841–850.

Ismail, H., Salleh, S.Z., Ahmad, Z., 2013. Properties of halloysite nanotubes-filled natural rubber prepared using different mixing methods. Mater. Des. 50, 790–797.

Jia, Z.X., Luo, Y.F., Guo, B.C., Yang, B.T., Du, M.L., Jia, D.M., 2009. Reinforcing and flame-retardant effects of halloysite nanotubes on LLDPE. Polym.-Plast. Technol. 48 (6), 607–613.

Jia, Z.X., Luo, Y.F., Yang, S.Y., Du, M.L., Guo, B.C., Jia, D.M., 2011. Styrene–butadiene rubber/halloysite nanotubes composites modified by epoxidized natural rubber. J. Nanosci. Nanotechnol. 11 (12), 10958–10962.

Joo, Y., Jeon, Y., Lee, S.U., Sim, J.H., Ryu, J., Lee, S., Lee, H., Sohn, D., 2012. Aggregation and stabilization of carboxylic acid functionalized halloysite nanotubes (HNT–COOH). J. Phys. Chem. C 116 (34), 18230–18235.

Joo, Y., Sim, J.H., Jeon, Y., Lee, S.U., Sohn, D., 2013. Opening and blocking the inner-pores of halloysite. Chem. Commun. 49 (40), 4519–4521.

Joussein, E., Petit, S., Churchman, J., Theng, B., Righi, D., Delvaux, B., 2005. Halloysite clay minerals: a review. Clay Miner. 40 (4), 383–426.

Joussein, E., Petit, S., Delvaux, B., 2007. Behavior of halloysite clay under formamide treatment. Appl. Clay Sci. 35 (1-2), 17–24.

Kiani, G., Dostali, M., Rostami, A., Khataee, A.R., 2011. Adsorption studies on the removal of Malachite Green from aqueous solutions onto halloysite nanotubes. Appl. Clay Sci. 54 (1), 34–39.

Kilislioglu, A., Bilgin, B., 2002. Adsorption of uranium on halloysite. Radiochim. Acta 90 (3), 155–160.

Kohyama, N., Fukushima, K., Fukami, A., 1978. Observation of hydrated form of tubular halloysite by an electron-microscope equipped with an environmental cell. Clay Clay Miner. 26 (1), 25–40.

Komori, Y., Matsumura, A., Itagaki, T., Sugahara, Y., Kuroda, K., 1999a. Preparation of a kaolinite-ε-caprolactam intercalation compound. Clay Sci. 11 (1), 47–55.

Komori, Y., Sugahara, Y., Kuroda, K., 1999b. Direct intercalation of poly(vinylpyrrolidone) into kaolinite by a refined guest displacement method. Chem. Mater. 11 (1), 3–6.

Komori, Y., Sugahara, Y., Kuroda, K., 1999c. Intercalation of alkylamines and water into kaolinite with methanol kaolinite as an intermediate. Appl. Clay Sci. 15 (1-2), 241–252.

Kristóf, J., Frost, R., Horváth, E., Kocsis, L., Inczédy, J., 1998. Thermoanalytical investigations on intercalated kaolinites. J. Therm. Anal. Calorim. 53 (2), 467–475.

Kuroda, K., Hiraguri, K., Komori, Y., Sugahara, Y., Mouri, H., Uesu, Y., 1999. An acentric arrangement of p-nitroaniline molecules between the layers of kaolinite. Chem. Commun. (22), 2253–2254.

Kuroda, Y., Ito, K., Itabashi, K., Kuroda, K., 2011. One-step exfoliation of kaolinites and their transformation into nanoscrolls. Langmuir 27 (5), 2028–2035.

Lecouvet, B., Horion, J., D'Haese, C., Bailly, C., Nysten, B., 2013a. Elastic modulus of halloysite nanotubes. Nanotechnology 24 (10).

Lecouvet, B., Sclavons, M., Bailly, C., Bourbigot, S., 2013b. A comprehensive study of the synergistic flame retardant mechanisms of halloysite in intumescent polypropylene. Polym. Degrad. Stab. 98 (11), 2268–2281.

Lecouvet, B., Sclavons, M., Bourbigot, S., Bailly, C., 2013c. Thermal and flammability properties of polyethersulfone/halloysite nanocomposites prepared by melt compounding. Polym. Degrad. Stab. 98 (10), 1993–2004.

Lee, S.Y., Kim, S.J., 2002. Adsorption of naphthalene by HDTMA modified kaolinite and halloysite. Appl. Clay Sci. 22 (1-2), 55–63.

Lee, S., Kim, Y.J., Moon, H.S., 1999. Phase transformation sequence from kaolinite to mullite investigated by an energy-filtering transmission electron microscope. J. Am. Ceram. Soc. 82 (10), 2841–2848.

Letaief, S., Detellier, C., 2007. Functionalized nanohybrid materials obtained from the interlayer grafting of aminoalcohols on kaolinite. Chem. Commun. (25), 2613–2615.

Levis, S.R., Deasy, P.B., 2003. Use of coated microtubular halloysite for the sustained release of diltiazem hydrochloride and propranolol hydrochloride. Int. J. Pharm. 253 (1-2), 145–157.

Li, C.P., Liu, J.G., Qu, X.Z., Yang, Z.Z., 2009. A general synthesis approach toward halloysite-based composite nanotube. J. Appl. Polym. Sci. 112 (5), 2647–2655.

Li, X., Yao, C., Lu, X., Hu, Z., Yin, Y., Ni, C., 2015. Halloysite–CeO_2–AgBr nanocomposite for solar light photodegradation of methyl orange Appl. Clay Sci. 104, 74–80.

Lipsicas, M., Straley, C., Costanzo, P.M., Giese Jr., R.F., 1985. Static and dynamic structure of water in hydrated kaolinites. II. The dynamic structure. J. Colloid Interface Sci. 107 (1), 221–230.

Liu, G., Kang, F., Li, B., Huang, Z., Chuan, X., 2006. Characterization of the porous carbon prepared by using halloysite as template and its application to EDLC. J. Phys. Chem. Solids 67 (5–6), 1186–1189.

Liu, M.X., Guo, B.C., Du, M.L., Cai, X.J., Jia, D.M., 2007. Properties of halloysite nanotube–epoxy resin hybrids and the interfacial reactions in the systems. Nanotechnology 18 (45).

Liu, M.X., Guo, B.C., Zou, Q.L., Du, M.L., Jia, D., 2008. Interactions between halloysite nanotubes and 2,5-bis(2-benzoxazolyl) thiophene and their effects on reinforcement of polypropylene/halloysite nanocomposites. Nanotechnology 19 (20).

Liu, M., Guo, B., Du, M., Chen, F., Jia, D., 2009a. Halloysite nanotubes as a novel β-nucleating agent for isotactic polypropylene. Polymer 50 (13), 3022–3030.

Liu, M., Guo, B., Du, M., Zou, Q., Jia, D., 2009b. Influence of hybrid fibrils of 2, 5-bis (2-benzoxazolyl) thiophene and halloysite nanotubes on the crystallization behaviour of polypropylene. J. Phys. D. Appl. Phys. 42 (7), 075306.

Liu, R.C., Zhang, B., Mei, D.D., Zhang, H.Q., Liu, J.D., 2011. Adsorption of methyl violet from aqueous solution by halloysite nanotubes. Desalination 268 (1-3), 111–116.

Liu, D., Yuan, P., Tan, D., Liu, H., Wang, T., Fan, M., Zhu, J., He, H., 2012. Facile preparation of hierarchically porous carbon using diatomite as both template and catalyst and methylene blue adsorption of carbon products. J. Colloid Interface Sci. 388 (1), 176–184.

Liu, D., Yuan, W., Yuan, P., Yu, W., Tan, D., Liu, H., He, H., 2013. Physical activation of diatomite-templated carbons and its effect on the adsorption of methylene blue (MB). Appl. Surf. Sci. 282, 838–843.

Liu, M., Jia, Z., Jia, D., Zhou, C., 2014. Recent advance in research on halloysite nanotubes–polymer nanocomposite. Prog. Polym. Sci. 39 (8), 1498–1525.

Lu, D., Chen, H.B., Wu, J.S., Chan, C.M., 2010. Direct measurements of the Young's modulus of a single halloysite nanotube using a transmission electron microscope with a bending stage. J. Nanosci. Nanotechnol. 11 (9), 7789–7793 (7785).

Luo, P., Zhao, Y.F., Zhang, B., Liu, J.D., Yang, Y., Liu, J.F., 2010. Study on the adsorption of Neutral Red from aqueous solution onto halloysite nanotubes. Water Res. 44 (5), 1489–1497.

Luo, P., Zhang, B., Zhao, Y.F., Wang, J.H., Zhang, H.Q., Liu, J.D., 2011. Removal of methylene blue from aqueous solutions by adsorption onto chemically activated halloysite nanotubes. Korean J. Chem. Eng. 28 (3), 800–807.

Lvov, Y., Price, R., Gaber, B., Ichinose, I., 2002. Thin film nanofabrication *via* layer-by-layer adsorption of tubule halloysite, spherical silica, proteins and polycations. Colloids Surf. A 198, 375–382.

Lvov, Y.M., Shchukin, D.G., Mohwald, H., Price, R.R., 2008. Halloysite clay nanotubes for controlled release of protective agents. ACS Nano 2 (5), 814–820.

Machado, G.S., Castro, K.A.D.F., Wypych, F., Nakagaki, S., 2008. Immobilization of metalloporphyrins into nanotubes of natural halloysite toward selective catalysts for oxidation reactions. J. Mol. Catal. A Chem. 283 (1-2), 99–107.

MacKenzie, K.J.D., Brown, I.W.M., Meinhold, R.H., Bowden, M.E., 1985. Outstanding problems in the kaolinite–mullite reaction sequence investigated by ^{29}Si and ^{27}Al solid-state nuclear magnetic resonance: I, Metakaolinite. J. Am. Ceram. Soc. 68 (6), 293–297.

Manevitch, O.L., Rutledge, G.C., 2004. Elastic properties of a single lamella of montmorillonite by molecular dynamics simulation. J. Phys. Chem. B 108 (4), 1428–1435.

Marney, D.C.O., Russell, L.J., Wu, D.Y., Nguyen, T., Cramm, D., Rigopoulos, N., Wright, N., Greaves, M., 2008. The suitability of halloysite nanotubes as a fire retardant for nylon 6. Polym. Degrad. Stab. 93 (10), 1971–1978.

Massiot, D., Dion, P., Alcover, J.F., Bergaya, F., 1995. ^{27}Al and ^{29}Si MAS NMR study of kaolinite thermal decomposition by controlled rate thermal analysis. J. Am. Ceram. Soc. 78 (11), 2940–2944.

Matsumura, A., Komori, Y., Itagaki, T., Sugahara, Y., Kuroda, K., 2001. Preparation of a kaolinite–nylon 6 intercalation compound. Bull. Chem. Soc. Jpn. 74 (6), 1153–1158.

Matusik, J., Wścisło, A., 2014. Enhanced heavy metal adsorption on functionalized nanotubular halloysite interlayer grafted with aminoalcohols. Appl. Clay Sci. 100, 50–59.

Matusik, J., Gawel, A., Bielanska, E., Osuch, W., Bahranowski, K., 2009. The effect of structural order on nanotubes derived from kaolin-group minerals. Clay Clay Miner. 57 (4), 452–464.

Mei, D.D., Zhang, B., Liu, R.C., Zhang, H.Q., Liu, J.D., 2011a. Preparation of stearic acid/halloysite nanotube composite as form-stable PCM for thermal energy storage. Int. J. Energy Res. 35 (9), 828–834.

Mei, D.D., Zhang, B., Liu, R.C., Zhang, Y.T., Liu, J.D., 2011b. Preparation of capric acid/halloysite nanotube composite as form-stable phase change material for thermal energy storage. Sol. Energy Mater. Sol. Cells 95 (10), 2772–2777.

Mellouk, S., Cherifi, S., Sassi, M., Marouf-Khelifa, K., Bengueddach, A., Schott, J., Khelifa, A., 2009. Intercalation of halloysite from Djebel Debagh (Algeria) and adsorption of copper ions. Appl. Clay Sci. 44 (3-4), 230–236.

Mitchell, M.J., Chen, C.S., Ponmudi, V., Hughes, A.D., King, M.R., 2012. E-selectin liposomal and nanotube-targeted delivery of doxorubicin to circulating tumor cells. J. Control. Release 160 (3), 609–617.

Mitra, G.B., 2013. Spiral structure of 7 Å halloysite: mathematical models. Clay Clay Miner. 61 (6), 499–507.

Motsi, T., Rowson, N.A., Simmons, M.J.H., 2009. Adsorption of heavy metals from acid mine drainage by natural zeolite. Int. J. Miner. Process. 92 (1–2), 42–48.

Ning, N.Y., Yin, Q.J., Luo, F., Zhang, Q., Du, R., Fu, Q., 2007. Crystallization behavior and mechanical properties of polypropylene/halloysite composites. Polymer 48 (25), 7374–7384.

Niu, J., Qiang, Y., Li, X., Liu, Z., Zhang, S., Feng, P., Ou, X., 2014. Morphology and orientation of curling of kaolinite layer in hydrate. Appl. Clay Sci. 101, 215–222.

Okada, K., ÕTsuka, N., Ossaka, J., 1986. Characterization of spinel phase formed in the kaolin–mullite thermal sequence. J. Am. Ceram. Soc. 69 (10), C251–C253.

Ouyang, J., Zhou, Z., Zhang, Y., Yang, H., 2014. High morphological stability and structural transition of halloysite (Hunan, China) in heat treatment. Appl. Clay Sci. 101, 16–22.

Papoulis, D., Tsolis-Katagas, P., Kalampounias, A.G., Tsikouras, B., 2009. Progressive formation of halloysite from the hydrothermal alteration of biotite and the formation mechanisms of anatase in altered volcanic rocks from Limnos Island, Northeast Aegean Sea, Greece. Clay Clay Miner. 57 (5), 566–577.

Pasbakhsh, P., Ismail, H., Fauzi, M.N.A., Abu Bakar, A., 2010. EPDM/modified halloysite nanocomposites. Appl. Clay Sci. 48 (3), 405–413.

Pasbakhsh, P., Churchman, G.J., Keeling, J.L., 2013. Characterisation of properties of various halloysites relevant to their use as nanotubes and microfibre fillers. Appl. Clay Sci. 74, 47–57.

Price, R.R., Gaber, B.P., Lvov, Y., 2001. In-vitro release characteristics of tetracycline HCl, khellin and nicotinamide adenine dineculeotide from halloysite; a cylindrical mineral. J. Microencapsul. 18 (6), 713–722.

Rao, K.M., Nagappan, S., Seo, D.J., Ha, C.-S., 2014. pH sensitive halloysite–sodium hyaluronate/poly(hydroxyethyl methacrylate) nanocomposites for colon cancer drug delivery. Appl. Clay Sci. 97–98, 33–42.

Rocha, J., Klinowski, J., 1990. ^{29}Si and ^{27}Al magic-angle-spinning NMR studies of the thermal transformation of kaolinite. Phys. Chem. Miner. 17 (2), 179–186.

Rooj, S., Das, A., Thakur, V., Mahaling, R.N., Bhowmick, A.K., Heinrich, G., 2010. Preparation and properties of natural nanocomposites based on natural rubber and naturally occurring halloysite nanotubes. Mater. Des. 31 (4), 2151–2156.

Shamsi, M.H., Geckeler, K.E., 2008. The first biopolymer-wrapped non-carbon nanotubes. Nanotechnology 19 (7).

Shchukin, D.G., Mohwald, H., 2007. Surface-engineered nanocontainers for entrapment of corrosion inhibitors. Adv. Funct. Mater. 17 (9), 1451–1458.

Shchukin, D.G., Sukhorukov, G.B., Price, R.R., Lvov, Y.M., 2005. Halloysite nanotubes as biomimetic nanoreactors. Small 1 (5), 510–513.

Shi, Y.F., Tian, Z., Zhang, Y., Shen, H.B., Jia, N.Q., 2011. Functionalized halloysite nanotube-based carrier for intracellular delivery of antisense oligonucleotides. Nanoscale Res. Lett. 6, 1–7.

Singh, B., 1996. Why does halloysite roll? — A new model. Clay Clay Miner. 44 (2), 191–196.

Singh, B., Gilkes, R.J., 1992. An electron-optical investigation of the alteration of kaolinite to halloysite. Clay Clay Miner. 40 (2), 212–229.

Singh, B., Mackinnon, I.D.R., 1996. Experimental transformation of kaolinite to halloysite. Clay Clay Miner. 44 (6), 825–834.

Smirnov, K.S., Bougeard, D., 1999. A molecular dynamics study of structure and short-time dynamics of water in kaolinite. J. Phys. Chem. B 103 (25), 5266–5273.

Smith, M.E., Neal, G., Trigg, M.B., Drennan, J., 1993. Structural characterization of the thermal transformation of halloysite by solid-state NMR. Appl. Magn. Reson. 4 (1-2), 157–170.

Sonuparlak, B., Sarikaya, M., Aksay, I.A., 1987. Spinel phase formation during the 980 °C exothermic reaction in the kaolinite-to-mullite reaction series. J. Am. Ceram. Soc. 70 (11), 837–842.

Suh, Y.J., Kil, D.S., Chung, K.S., Abdullayev, E., Lvov, Y.M., Mongayt, D., 2011. Natural nanocontainer for the controlled delivery of glycerol as a moisturizing agent. J. Nanosci. Nanotechnol. 11 (1), 661–665.

Szczepanik, B., Słomkiewicz, P., Garnuszek, M., Czech, K., 2014. Adsorption of chloroanilines from aqueous solutions on the modified halloysite. Appl. Clay Sci. 101, 260–264.

Takenawa, R., Komori, Y., Hayashi, S., Kawamata, J., Kuroda, K., 2001. Intercalation of nitroanilines into kaolinite and second harmonic generation. Chem. Mater. 13 (10), 3741–3746.

Tan, D., Yuan, P., Annabi-Bergaya, F., Yu, H., Liu, D., Liu, H., He, H., 2013. Natural halloysite nanotubes as mesoporous carriers for the loading of ibuprofen. Microporous Mesoporous Mater. 179, 89–98.

Tan, D., Yuan, P., Annabi-Bergaya, F., Liu, D., He, H., 2014a. High-capacity loading of 5-fluorouracil on the methoxy-modified kaolinite. Appl. Clay Sci. 100, 60–65.

Tan, D., Yuan, P., Annabi-Bergaya, F., Liu, D., Wang, L., Liu, H., He, H., 2014b. Loading and in vitro release of ibuprofen in tubular halloysite. Appl. Clay Sci. 96, 50–55.

Tan, D., Yuan, P., Annabi-Bergaya, F., Liu, D., He, H., 2015. Methoxy-modified kaolinite as a novel carrier for high-capacity loading and controlled-release of the herbicide amitrole. Sci. Rep. U.K. 5, 8870.

Tang, Y.H., Deng, S.Q., Ye, L., Yang, C., Yuan, Q.A., Zhang, J.N., Zhao, C.B., 2011. Effects of unfolded and intercalated halloysites on mechanical properties of halloysite–epoxy nanocomposites. Compos. Part A Appl. Sci. 42 (4), 345–354.

Thakur, P., Kool, A., Bagchi, B., Das, S., Nandy, P., 2014. Enhancement of β phase crystallization and dielectric behavior of kaolinite/halloysite modified poly(vinylidene fluoride) thin films. Appl. Clay Sci. 99, 149–159.

Tonlé, I.K., Diaco, T., Ngameni, E., Detellier, C., 2007. Nanohybrid kaolinite-based materials obtained from the interlayer grafting of 3-aminopropyltriethoxysilane and their potential use as electrochemical sensors. Chem. Mater. 19 (26), 6629–6636.

Tonlé, I.K., Letaief, S., Ngameni, E., Detellier, C., 2009. Nanohybrid materials from the grafting of imidazolium cations on the interlayer surfaces of kaolinite. Application as electrode modifier. J. Mater. Chem. 19 (33), 5996–6003.

Tunney, J.J., Detellier, C., 1996. Chemically modified kaolinite. Grafting of methoxy groups on the interlamellar aluminol surface of kaolinite. J. Mater. Chem. 6 (10), 1679–1685.

Vassallo, A.M., Coleclarke, P.A., Pang, L.S.K., Palmisano, A.J., 1992. Infrared-emission spectroscopy of coal minerals and their thermal transformations. Appl. Spectrosc. 46 (1), 73–78.

Veerabadran, N.G., Price, R.R., Lvov, Y.M., 2007. Clay nanotubes for encapsulation and sustained release of drugs. Nano 2 (2), 115–120.

Veerabadran, N.G., Mongayt, D., Torchilin, V., Price, R.R., Lvov, Y.M., 2009. Organized shells on clay nanotubes for controlled release of macromolecules. Macromol. Rapid Commun. 30 (2), 99–103.

Vergaro, V., Abdullayev, E., Lvov, Y.M., Zeitoun, A., Cingolani, R., Rinaldi, R., Leporatti, S., 2010. Cytocompatibility and uptake of halloysite clay nanotubes. Biomacromolecules 11 (3), 820–826.

Vergaro, V., Lvov, Y.M., Leporatti, S., 2012. Halloysite clay nanotubes for resveratrol delivery to cancer cells. Macromol. Biosci. 12 (9), 1265–1271.

Viseras, M.T., Aguzzi, C., Cerezo, P., Viseras, C., Valenzuela, C., 2008. Equilibrium and kinetics of 5-aminosalicylic acid adsorption by halloysite. Microporous Mesoporous Mater. 108 (1-3), 112–116.

Viseras, M.-T., Aguzzi, C., Cerezo, P., Cultrone, G., Viseras, C., 2009. Supramolecular structure of 5-aminosalycilic acid/halloysite composites. J. Microencapsul. 26 (3), 279–286.

Wang, A.P., Kang, F., Huang, Z.H., Guo, Z., 2006. Preparation of porous carbons from halloysite–sucrose mixtures. Clay Clay Miner. 54 (4), 485–490.

Wang, A., Kang, F., Huang, Z., Guo, Z., Chuan, X., 2008. Synthesis of mesoporous carbon nanosheets using tubular halloysite and furfuryl alcohol by a template-like method. Microporous Mesoporous Mater. 108 (1–3), 318–324.

Wang, J.H., Zhang, X.A., Zhang, B., Zhao, Y.F., Zhai, R., Liu, J.D., Chen, R.F., 2010. Rapid adsorption of Cr (VI) on modified halloysite nanotubes. Desalination 259 (1-3), 22–28.

Wang, Y., Zhang, X., Wang, Q., Zhang, B., Liu, J., 2014a. Continuous fixed bed adsorption of Cu(II) by halloysite nanotube–alginate hybrid beads: an experimental and modelling study. Water Sci. Technol. 70 (2), 192–199.

Wang, Q., Zhang, J., Zheng, Y., Wang, A., 2014b. Adsorption and release of ofloxacin from acid- and heat-treated halloysite. Colloids Surf. B 113, 51–58.

White, R.D., Bavykin, D.V., Walsh, F.C., 2012. The stability of halloysite nanotubes in acidic and alkaline aqueous suspensions. Nanotechnology 23 (6).

Xie, Y.F., Qian, D.Y., Wu, D.L., Ma, X.F., 2011. Magnetic halloysite nanotubes/iron oxide composites for the adsorption of dyes. Chem. Eng. J. 168 (2), 959–963.

Yah, W.O., Takahara, A., Lvov, Y.M., 2012a. Selective modification of halloysite lumen with octadecylphosphonic acid: new inorganic tubular micelle. J. Am. Chem. Soc. 134 (3), 1853–1859.

Yah, W.O., Xu, H., Soejima, H., Ma, W., Lvov, Y., Takahara, A., 2012b. Biomimetic dopamine derivative for selective polymer modification of halloysite nanotube lumen. J. Am. Chem. Soc. 134 (29), 12134–12137.

Yang, S., Yuan, P., He, H., Qin, Z., Zhou, Q., Zhu, J., Liu, D., 2012. Effect of reaction temperature on grafting of γ-aminopropyl triethoxysilane (APTES) onto kaolinite. Appl. Clay Sci. 62–63, 8–14.

Ye, Y.P., Chen, H.B., Wu, J.S., Ye, L., 2007. High impact strength epoxy nanocomposites with natural nanotubes. Polymer 48 (21), 6426–6433.

Yiu, H.H.P., Botting, C.H., Botting, N.P., Wright, P.A., 2001. Size selective protein adsorption on thiol-functionalised SBA-15 mesoporous molecular sieve. Phys. Chem. Chem. Phys. 3 (15), 2983–2985.

Yuan, P., Southon, P.D., Liu, Z., Green, M.E.R., Hook, J.M., Antill, S.J., Kepert, C.J., 2008. Functionalization of halloysite clay nanotubes by grafting with γ-aminopropyltriethoxysilane. J. Phys. Chem. C 112 (40), 15742–15751.

Yuan, P., Fan, M., Yang, D., He, H., Liu, D., Yuan, A., Zhu, J., Chen, T., 2009. Montmorillonite-supported magnetite nanoparticles for the removal of hexavalent chromium [Cr(VI)] from aqueous solutions. J. Hazard. Mater. 166 (2–3), 821–829.

Yuan, P., Liu, D., Fan, M., Yang, D., Zhu, R., Ge, F., Zhu, J., He, H., 2010. Removal of hexavalent chromium [Cr(VI)] from aqueous solutions by the diatomite-supported/unsupported magnetite nanoparticles. J. Hazard. Mater. 173 (1–3), 614–621.

Yuan, P., Tan, D.Y., Annabi-Bergaya, F., Yan, W.C., Fan, M.D., Liu, D., He, H.P., 2012a. Changes in structure, morphology, porosity, and surface activity of mesoporous halloysite nanotubes under heating. Clay Clay Miner. 60 (6), 561–573.

Yuan, P., Southon, P.D., Liu, Z.W., Kepert, C.J., 2012b. Organosilane functionalization of halloysite nanotubes for enhanced loading and controlled release. Nanotechnology 23 (37).

Yuan, P., Tan, D., Annabi-Bergaya, F., Yan, W., Liu, D., Liu, Z., 2013. From platy kaolinite to aluminosilicate nanoroll *via* one-step delamination of kaolinite: effect of the temperature of intercalation. Appl. Clay Sci. 83–84, 68–76.

Zhai, R., Zhang, B., Liu, L., Xie, Y.D., Zhang, H.Q., Liu, J.D., 2010. Immobilization of enzyme biocatalyst on natural halloysite nanotubes. Catal. Commun. 12 (4), 259–263.

Zhang, L., Liu, P., 2008. Facile fabrication of uniform polyaniline nanotubes with tubular aluminosilicates as templates. Nanoscale Res. Lett. 3 (8), 299–302.

Zhang, Y., Fu, L.J., Yang, H.M., 2012a. Insights into the physicochemical aspects from natural halloysite to silica nanotubes. Colloids Surf. A 414, 115–119.

Zhang, A.B., Pan, L., Zhang, H.Y., Liu, S.T., Ye, Y., Xia, M.S., Chen, X.G., 2012b. Effects of acid treatment on the physico-chemical and pore characteristics of halloysite. Colloids Surf. A 396, 182–188.

Zhang, Y., Gao, R., Liu, M., Yan, C., Shan, A., 2014. Adsorption of modified halloysite nanotubes in vitro and the protective effect in rats exposed to zearalenone. Arch. Anim. Nutr. 68 (4), 320–335.

Zhao, M.F., Liu, P., 2008. Adsorption behavior of methylene blue on halloysite nanotubes. Microporous Mesoporous Mater. 112 (1-3), 419–424.

Zhao, J., Deng, C.L., Du, S.L., Chen, L., Deng, C., Wang, Y.Z., 2014. Synergistic flame-retardant effect of halloysite nanotubes on intumescent flame retardant in LDPE. J. Appl. Polym. Sci. 131 (7).

Zheng, Y.A., Wang, A.Q., 2010. Enhanced adsorption of ammonium using hydrogel composites based on chitosan and halloysite. J. Macromol. Sci. A 47 (1), 33–38.